2008

SCHOTTKY DIODES ON COPPER PHTHALOCYANINE NANOWIRE ARRAYS EMBEDDED IN POROUS ALUMINA TEMPLATES

Goutam Chintakula
University of Kentucky, goutamonline@uky.edy

ABSTRACT OF THESIS

SCHOTTKY DIODES ON COPPER PHTHALOCYANINE NANOWIRE ARRAYS EMBEDDED IN POROUS ALUMINA TEMPLATES

Vertically aligned nanowire arrays of copper phthalocyanine (CuPc) and CuPc-Al Schottky diodes, of controllable diameter and length were fabricated by cathodic electrodeposition of CuPc into anodized alumina (AAO) templates, followed by annealing at 300 ºC in Argon. AAO over Aluminum tape and that over ITO-glass were both used as starting templates for the device fabrication. Depending on the dimensions of the starting AAO template, diameters of CuPc nanowires ranged from 30 nm to 40 nm and the lengths ranged from 500 nm to 1 μm. The temperature dependence of the phase and the absorption spectrum of the nanowires are reported. The electrodeposited nanowires (as prepared) had the preferred crystallite orientation of the α-phase. ITO formed the ohmic contact and Schottky contacts were formed between CuPc and aluminum. Insertion of a thin layer of PEDOT:PSS between CuPc nanowires and the ITO electrode improved the contact and reduced the series resistance by an order of magnitude. Schottky diodes were characterized and analyzed at room temperature and at cryogenic temperatures.

KEYWORDS: Schottky diode, Copper Phthalocyanine (CuPc), Nanowires, Anodic Aluminum Oxide (AAO), Electrodeposition.

Goutam Chintakula

October 24th 2008

SCHOTTKY DIODES ON COPPER PHTHALOCYANINE NANOWIRE ARRAYS EMBEDDED IN POROUS ALUMINA TEMPLATES

By

Goutam Chintakula

_____

(Dr. Vijay P Singh)

_____

(Dr. YuMing Zhang)

_____

RULES FOR THE USE OF THESIS

Unpublished thesis submitted for the Master's degree and deposited in the University of Kentucky Library are as a rule open for inspection, but are to be used only with due regard to the rights of the authors. Bibliographical references may be noted, but quotations or summaries of parts may be published only with the permission of the author, and with the usual scholarly acknowledgments.

Extensive copying or publication of the dissertation in whole or in part also requires the consent of the Dean of the Graduate School of the University of Kentucky.

A library that borrows this dissertation for use by its patrons is expected to secure the signature of each user.

Name Date

_____

_____

_____

_____

_____

_____

_____

_____

_____

_____

THESIS

Goutam Chintakula

The Graduate School

University of Kentucky

2008

SCHOTTKY DIODES ON COPPER PHTHALOCYANINE NANOWIRE ARRAYS EMBEDDED IN POROUS ALUMINA TEMPLATES

THESIS

A thesis submitted in partial fulfillment of the requirements for the degree of Master of Science in Electrical Engineering in the College of Engineering at the University of Kentucky

By

Goutam Chintakula

Lexington, Kentucky

Director: Dr. Vijay P. Singh, Professor

Electrical and Computer Engineering

Lexington, Kentucky

2008

DEDICATION

To Parents, sister and all my family members

ACKNOWLEDGEMENTS

I would like to take this opportunity to express my sincere thanks and heartfelt gratitude to my academic advisor and thesis chair Dr. Vijay Singh for his guidance and support throughout my thesis. I am very thankful for his constant encouragement during the thesis. I also would like to extend my thanks to Dr. Todd Hastings and Dr. J. Robert Heath for serving on my thesis committee and providing me with invaluable comments and suggestions for improving this thesis.

I extend my deepest gratitude and heartfelt thanks to Dr. Suresh Rajaputra and Dr. Sovannary Phok without whom the thesis would have never taken its present shape. I am greatly indebted for their technical support throughout my thesis. I would also like to thank other members of the group for their technical assistance and support.

My parents and my friends have been great sources of support throughout my studies in the USA and before that. They have had to live with many years of separation from me while I have been involved in my academic pursuits in the USA. My friends have given me a lot of love without which this work would not have been possible.

Table of Contents

List of Tables

List of figures

List of Files

1. Thesis pdf.....……4.78MB

1. Introduction

For the past forty years inorganic silicon and gallium arsenide semiconductors, silicon dioxide insulators, and metals such as aluminum and copper have been the backbone of the semiconductor industry. However, there has been a growing research effort in "organic electronics" to improve the semiconducting, conducting, and light emitting properties of organics (polymers, oligomers) and hybrids (organic–inorganic composites) through novel synthesis and self-assembly techniques. Performance improvements, coupled with the ability to process these active materials at low temperatures over large areas on materials such as plastic or paper, may provide unique technologies and generate new applications and form factors to address the growing needs for computing and enhanced connectivity.

The growing need for more efficient and reliable power production has triggered the research on Nano-based solar cells. Organic solar cells have recently been proposed as a key for energy supply because they are compatible with plastics, are flexible and can a cover a large area. Organic materials also have the key advantage of simple and low-temperature thin-film processing through inexpensive techniques such as spin coating, ink-jet printing, stamping, sputtering, E-beam evaporation, thermal evaporation etc. In addition, the flexibility of organic chemistry enables the formation of organic molecules with useful luminescent, photoelectric and conducting properties. The ability of these materials to transport charge (holes and electrons) due to the π-orbital overlap of neighboring molecules provides their semiconducting and conducting properties. While very promising with regard to processing, cost, and weight considerations, organic compounds generally have a number of disadvantages, including poor thermal and mechanical stability. In addition, while electrical transport in organic materials has improved, the room temperature mobility is fundamentally limited by the weak van der Waals interactions between organic molecules as opposed to the stronger covalent and ionic forces found in extended inorganic systems [1].

A phthalocyanine is a macrocyclic compound having an alternating nitrogen atom-carbon atom ring structure. A macrocycle is, as defined by IUPAC, "a cyclic macromolecule or a macromolecular cyclic portion of a molecule." The molecule is able to coordinate hydrogen and metal cations in its center by coordinate bonds with the four isoindole nitrogen atoms. Most of the elements have been found to be able to coordinate to the phthalocyanine macrocycle. Therefore, a variety of phthalocyanine complexes exist [2].

The Figure 1 below shows that a phthalocyanine macrocycle consists of four identical corners. A synthesis strategy, therefore, starts from molecules which correspond to these corners. Such molecules are derivatives of phthalic acid. Several of these starting materials are shown in the Figure 2 below [reiterated from Wikipedia.com].

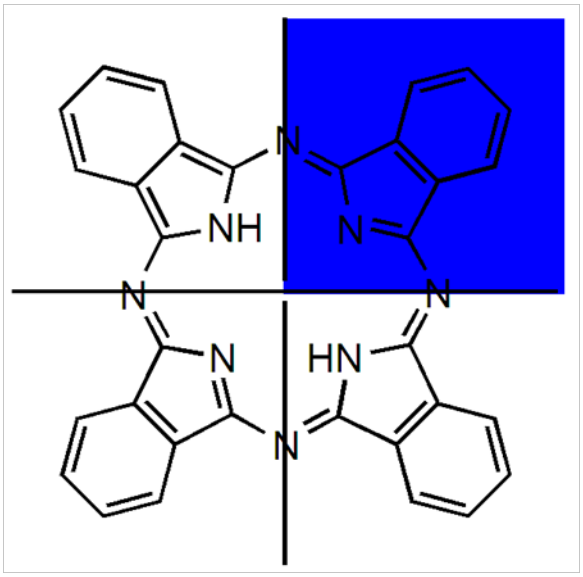

Figure 1: Strategy for the synthesis of phthalocyanines [Ref. 2]

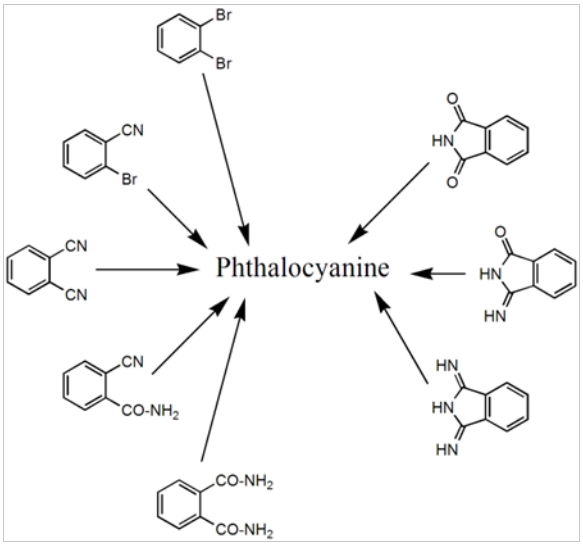

Figure 2: Typical starting materials for the synthesis of phthalocyanines [Ref. 2]

The phthalocyanine is a blue-colored dye molecule with high chemical and physical stability. They have several polymorphic forms, and the crystal structures of metal-free and

various metal derivatives are different. Metal-free phthalocyanine has at least four polymorphs: α, β, τ, and χ. They have two main electronic absorption regions: the Q band, generally in the range 600–700nm, and the Soret band, in the range 300–400nm [18]. In the solid state these bands generally split into two components due to excitonic coupling between overlapping molecules. The effect of this splitting is strongly dependent on the relative orientation and separation of neighboring molecules, so that different polymorphic forms have very different absorption spectra.

Metal phthalocyanine (MPc) is an excellent organic semiconductor and its optical and electrical properties have long been studied extensively due to its potential applications to xerography, gas sensors, electronic and photovoltaic devices including field effect transistors and solar cells. MPc is also expected to be a candidate material for optical detectors with more tunable absorption band and lower cost than its inorganic counterparts. In most of these applications, the sensitivity or efficiency of the devices is crucial and usually proportional to the total surface area of the MPc. Nanowire arrays can offer a larger surface area compared to the films or bulk materials, leading to the enhanced photoelectric conversion efficiency. Furthermore, the nanostructured arrays, because of their special quantum size effect, own a number of unique physical and electronic properties that endow them with new and important activities in the nanotechnology science.

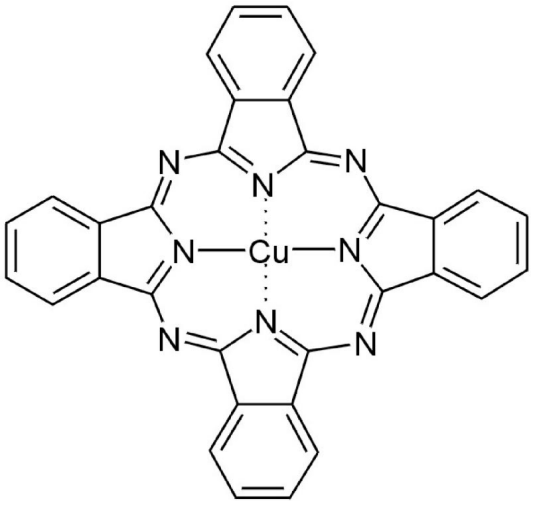

Figure 3: Schematic representation of the molecular structure of CuPc [Ref. 31]

Copper phthalocyanine (CuPc) is one of those MPc organic semiconductors that are finding applications in a wide variety of optoelectronic devices including light emitting diodes [3-

5] and solar cells [6-13]. Its molecular structure is shown in Figure 3. Its molecular formula is $\mathbf{C_{32}H_{16}CuN_8}$ and has a molecular mass of about **576.1**. It has five polymorphs [18]: α, β, γ, δ, and ε. The monoclinic α and β forms differ in the angle between the stacking axis and the normal to the molecular plane, which is 26.5° in the former and 45.8° in the latter.

Earlier, high open circuit voltages (V_{oc}) in a single organic heterojunction solar cell involving CuPc were reported [11-13]. However short circuit current densities (J_{sc}) in these cells as in organic semiconductor solar cells (OSSCs), in general, are low. The major reason for low J_{sc} in OSSCs is the rather small exciton diffusion length of a few nm. Nanowire cell designs and use of ordered structures offer a way out of this serious limitation and thus a path to high efficiency OSSCs [14-15]. These nano-structures have many advantages. First, they are relatively easy to model. Second, the dimensions can be controlled to ensure that every spot of the 2 semiconductors are within the exciton diffusion length of the interface and third, the presence of straight conducting paths to the electrodes minimizes recombination [28].

Template based fabrication methods, typically employing electrodeposition, provide a direct way to vary the diameter and length of pores and chemical composition of nanowires embedded in them. Thus nano-template based technology provides a platform for not only achieving higher performance in solar cells and other optoelectronic devices, but also for performing systematic studies of the effects of size on the characteristics of these nanowires. The method is relatively simple and adaptable to large scale production. As a major step in the development of this technology, CuPc-Al Schottky diodes in a nanowire mode were fabricated and their characteristics were studied.

This work focuses over the fabrication of CuPc-Al Schottky diodes in a nanowire mode using AAO templates. Device and material characteristics are discussed. Chapter 2 describes the basic theory behind Metal-Semiconductor junctions and their characteristics, and organic-based photovoltaics. The third chapter discusses the experimental details of the CuPc-Al device fabrication and the forth chapter illustrates the results and discusses the observations made. The last chapter summarizes the thesis with the conclusions drawn and presents suggestions for future research work.

2. Theory

2.1 Metal-Semiconductor Junctions

2.1.1 Schottky Contacts

P-n junction diodes are the basic non-linear devices being used all over the world. By simply forming an appropriate metal-semiconductor contact, many of the useful properties of a p-n junction can be achieved. They are particularly useful when high-speed rectification is required. Consider a metal with work function $q\Phi_m$. That is energy of $q\Phi_m$ is required to remove an electron at the Fermi level to the vacuum outside the metal. When negative charges are brought near the metal surface, positive (image) charges are induced in the metal. When this image force is combined with an applied electric field, the effective work function is somewhat reduced. Such barrier lowering is called the Schottky effect and rectifying contacts are generally referred to as Schottky barrier diodes.

When the metal is brought in contact with a semiconductor having a work function $q\Phi_s$, charge transfer occurs until the Fermi levels align at equilibrium. When $\Phi_m > \Phi_s$, the semiconductor Fermi level is initially higher than that of the metal before contact is made as shown in Figure 4.

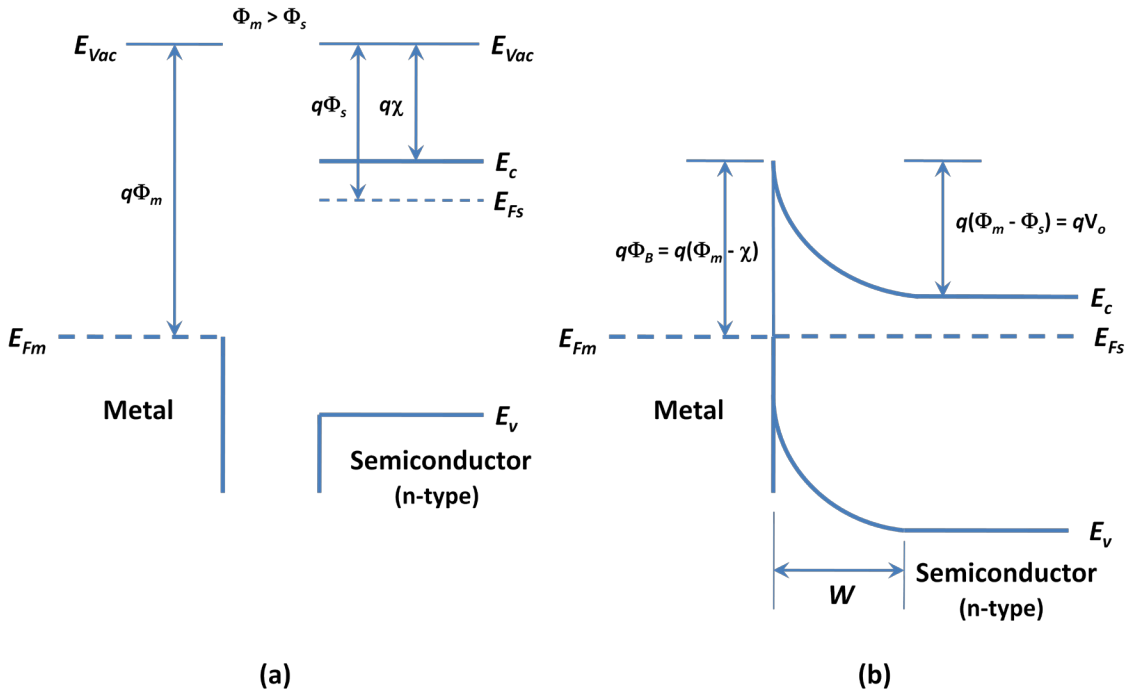

Figure 4: A Schottky barrier between a metal and an n-type semiconductor with $\Phi_m > \Phi_s$; (a) band diagrams before joining; (b) equilibrium band diagram for the junction

The electrostatic potential of the semiconductor must be raised relative to that of the metal in order to align the two Fermi levels. In the n-type semiconductor of Figure 4, after the contact has been made, a depletion region W is formed near the junction. The positive charge due to uncompensated donor ions within W matches the negative charge on the metal. The electric field and the bending of the bands within W are similar to effects for p-n junctions.

At equilibrium, a contact potential of V_o is formed at the junction. This potential prevents further electron diffusion from the semiconductor conduction band into the metal. The contact potential is given by the difference in the work function potentials $\Phi_m - \Phi_s$. The potential barrier height, Φ_B, for electron injection from the metal into the semiconductor conduction band is $\Phi_m - \chi$, where $q\chi$ is the electron affinity measured from the vacuum level to the semiconductor conduction band edge. By applying either forward or reverse-bias voltage, the equilibrium potential difference V_o can be decreased or increased as in the p-n junction.

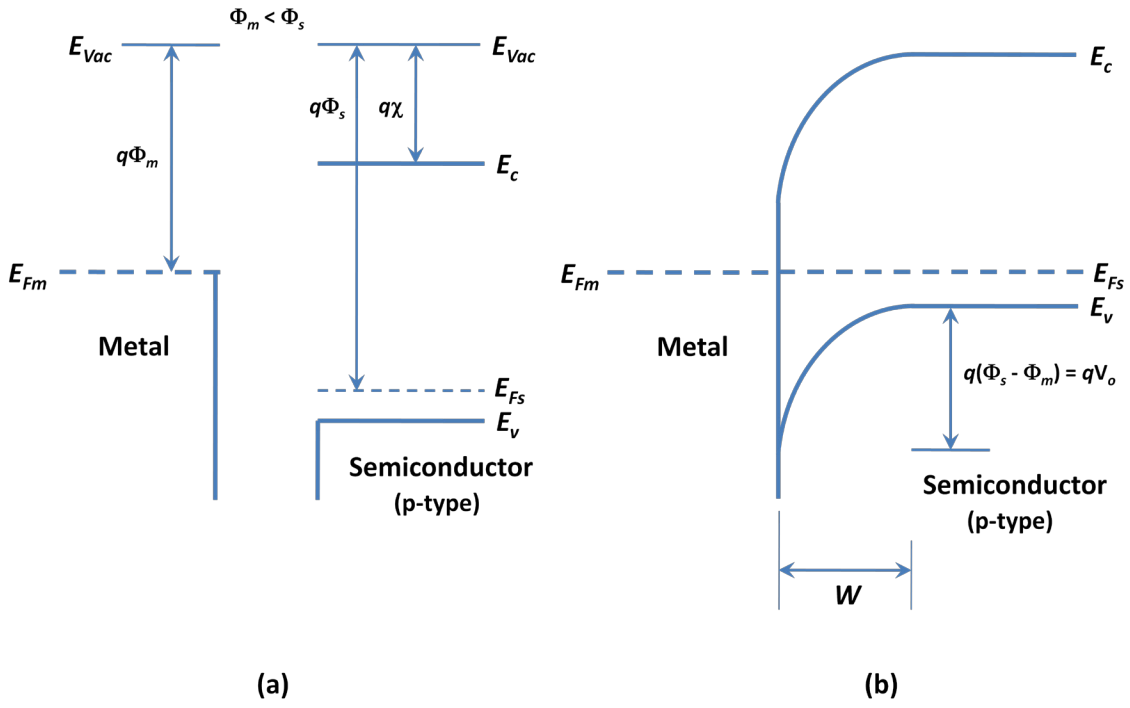

Figure 5: A Schottky barrier between a metal and a p-type semiconductor with $\Phi_m < \Phi_s$; (a) band diagrams before joining; (b) equilibrium band diagram for the junction

Figure 5 illustrates a Schottky barrier on a p-type semiconductor, with $\Phi_m < \Phi_s$. In this case aligning the Fermi levels at equilibrium requires a positive charge on the metal side and a negative charge on the semiconductor side of the junction. The negative charge is accommodated

by a depletion region W in which ionized acceptors are left uncompensated by holes. The potential barrier V_o retarding hole diffusion from the semiconductor to the metal is Φ_s - Φ_m, and as before this potential can be raised or lowered by the application of voltage across the junction.

2.1.2 Ohmic Contacts

An ohmic contact refers to the contact between a metal and a semiconductor to allow carriers to flow in and out of the semiconductor. An ideal ohmic contact must be capable of delivering the required current with no voltage drop between the semiconductor and the metal. In real life, therefore, an ohmic contact must have a contact resistance that is as small as possible, to make it negligible in comparison to the bulk resistance of the semiconductor.

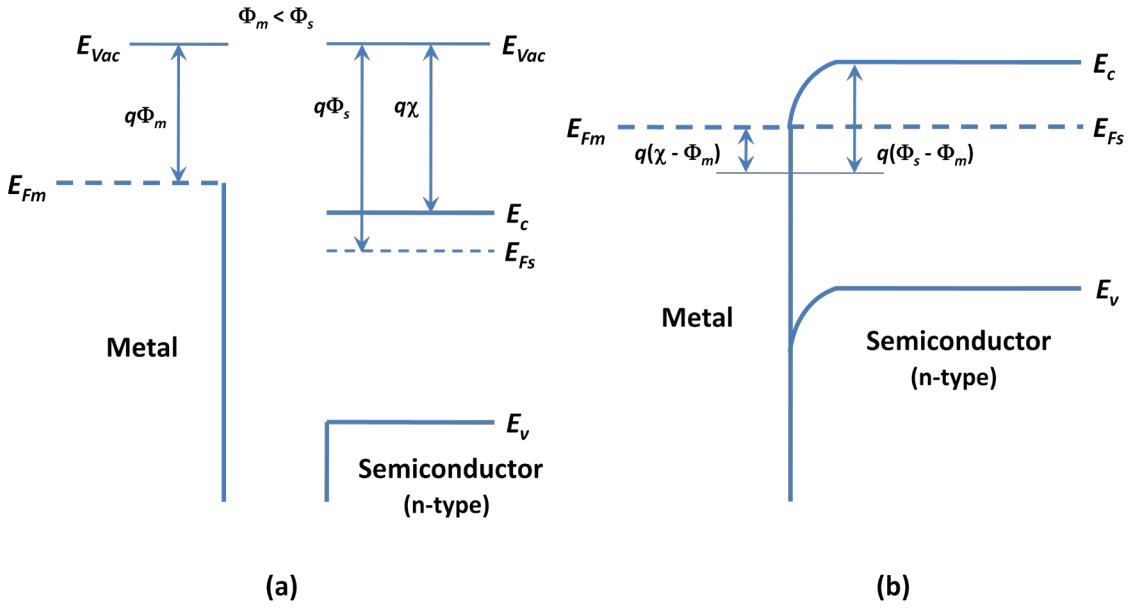

Figure 6: An Ohmic contact between a metal and an n-type semiconductor with $\Phi_m < \Phi_s$; (a) band diagrams before joining; (b) equilibrium band diagram for the junction

Ideal metal-semiconductor contacts are ohmic when the charge induced in the semiconductor in aligning the Fermi levels is provided by majority carriers. For example, in the $\Phi_m < \Phi_s$ case of Figure 6, the Fermi levels are aligned at equilibrium by transferring electrons from the metal to the semiconductor. This raises the semiconductor electron energies relative to the metal at equilibrium. In this case the barrier to the electron flow between the metal and the semiconductor is small and easily overcome by a small voltage. Similarly, the case $\Phi_m > \Phi_s$ (p-type) results in easy hole flow across the junction. Figure 7 illustrates this.

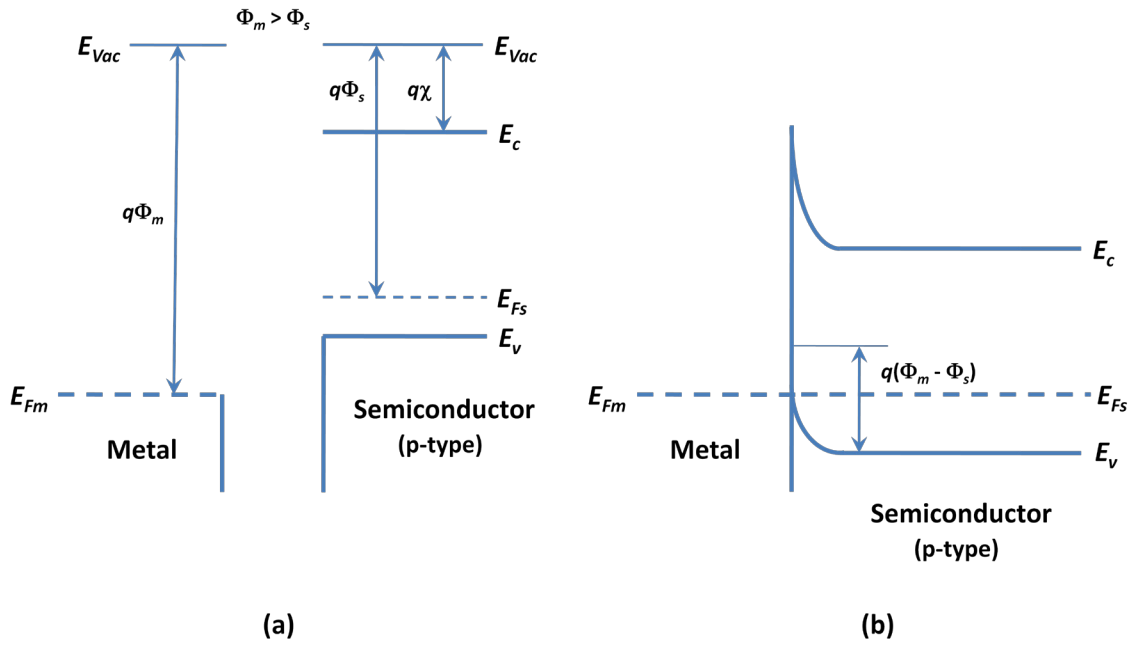

Figure 7: An Ohmic contact between a metal and a p-type semiconductor with $\Phi_m > \Phi_s$; (a) band diagrams before joining; (b) equilibrium band diagram for the junction

2.1.3 Schottky Diode characteristics

Since the rectifying contact behaves the same way as a p-n junction diode, the diode equation holds good for the *I-V* characteristics of the metal-semiconductor junction. The diode equation is given by

$$I = I_0(e^{\frac{qV}{kT}} - 1)$$

where I_o is the reverse saturation current, V is the applied voltage, k is the Boltzmann's constant and T is the temperature. The reverse saturation current, I_o, is given by

$$I_0 = ABT^2(e^{-\frac{q\Phi B}{kT}})$$

where B is effective Richardson constant.

When a forward-bias voltage V is applied to the Schottky barrier of Figure 4, the contact potential is reduced from V_o to $V_o - V$ as shown in Figure 8(a). As a result, electrons in the semiconductor conduction band can diffuse across the depletion region to the metal. This gives rise to forward current through the junction. Conversely, a reverse bias increases the barrier to $V_o + V_r$, and electron flow from semiconductor to metal becomes negligible (Figure 8(b)). Here, the forward current is due to the injection of majority carriers from the semiconductor into the metal.

The absence of minority carrier injection and the associated storage delay time is an important feature of Schottky barrier diodes. Their high-frequency properties and switching speed are therefore generally better than typical p-n junctions.

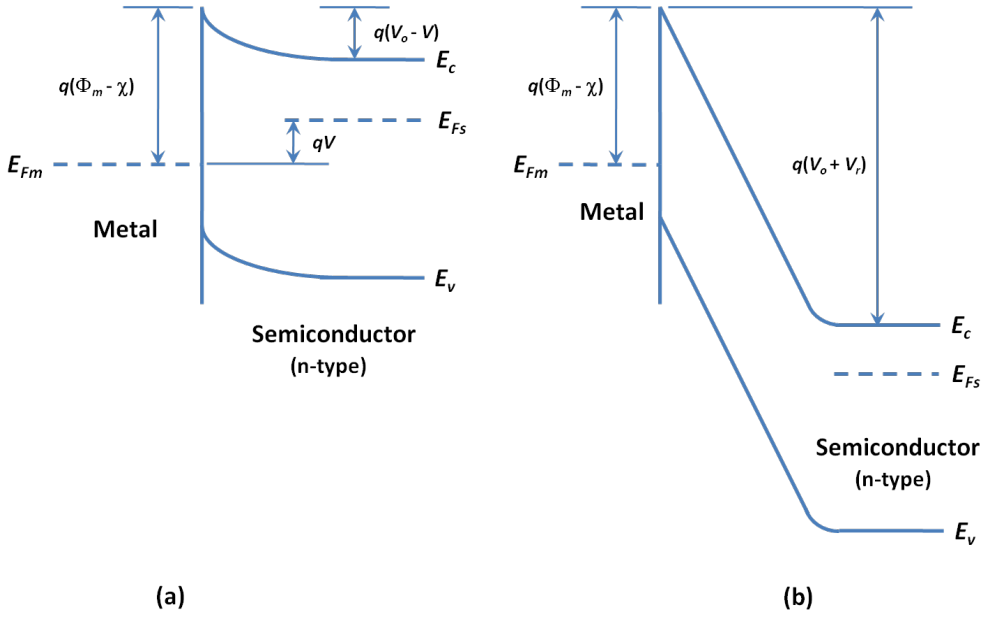

Figure 8: Biasing a Schottky barrier; (a) Forward bias, (b) Reverse bias

2.2 Organic-Based Photovoltaics

As discussed in Chapter 1, organic photovoltaics offer the long-term potential of achieving the goal of a PV technology that is economically viable for large-scale power generation. Organic-based photovoltaics (OPVs) have many advantages. They are inexpensive, have very high optical absorption coefficients that permit the use of films with thicknesses of only several hundred nanometers; are compatible with plastic substrates and can be fabricated using high-throughput, low-temperature approaches. Such low-temperature, and therefore low-energy-consuming, techniques require less capital investment than fabrication techniques for Si-based devices. In addition, the possibility of using flexible plastic substrates in an easily scalable, high-speed printing process can reduce the costs for OPVs to make them competitive with inorganic thin-film technologies. Thus, if efficiencies are comparable or even slightly lower than existing technologies, there may be compelling cost arguments favoring OPVs.

One of the main issues faced by the organic electronics community in general is the stability of the organic materials. Organic materials tend to degrade because of many reasons;

changes in morphology, loss of interfacial adhesion, and interdiffusion of components [29], a few to mention. Thus, careful design and materials engineering is required to substantially improve device lifetimes. There are a number of other key aspects of organic materials. They allow for alteration of a wide range of properties, including molecular weight, bandgap, molecular orbital energy levels, wetting properties, structural properties (rigidity, conjugation length, molecule- to-molecule interactions, etc.), and doping. This ability to design and synthesize molecules and then integrate them into organic–organic and inorganic–organic composites provides a unique pathway in the design of materials for novel devices. Additionally, the ability to alter the color of the device, allows us to fabricate devices on flexible substrates, and potentially print them in any pattern.

Organic electronic materials are conjugated solids where both optical absorption and charge transport are dominated by partly delocalized π and π^* orbitals. They can be broadly classified as either small molecules, with molecular weights of less than a few thousand atomic mass units (amu), or polymers, with molecular weights greater than 10,000 amu. Organic photovoltaic materials differ from inorganic semiconductors in many important aspects. In the case of organic materials, excitons are strongly bound and do not spontaneously dissociate into separate charges. Dissociation requires an input energy of ~100 meV [27] compared to a few meV for a crystalline semiconductor. This means that carrier generation does not necessarily result from the absorption of light. Charge transport proceeds by hopping between localized states, rather than transport within a band, which results in low mobilities. Also, due to the high degree of disorder in organic solids, their mobilities are low. The spectral range of optical absorption is relatively narrow compared to the solar spectrum. Absorption coefficients are high so that high optical densities can be achieved with films less than 100 nm thick. Many organic materials are unstable in the presence of oxygen or water as discussed previously. The intermolecular van der Waals forces in organic solids are weak compared to bonds in inorganic crystals and much weaker than the intramolecular bonds. As a consequence, all electronic states are localized on single molecules and do not form bands. The optical excitations are mainly due to the π to π^* transitions. Most conjugated solids absorb in the blue or green; absorption in the red or infrared is harder to achieve.

These properties impose some constraints on organic photovoltaic devices.

(a) A strong driving force should be present to break up the photogenerated excitons.
(b) Low charge carrier mobilities limit the useful thickness of devices.

(c) Limited light absorption across the solar spectrum limits the photocurrent.

(d) Very thin devices mean interference effects can be important.

(e) Photocurrent is sensitive to temperature through hopping transport.

[Note: Most of the theory in section 2.2 has been taken from the references 29 and 30]

2.3 Device Structure and operation

Two types of device structures were investigated as shown in Figures 9-10. In both cases Aluminum acts as a cathode and Indium Tin Oxide (ITO) as an anode. In Type-I devices, CuPc nanowires stand over the cathode, Al, inside the alumina (Al_2O_3) template while in Type-II devices, CuPc nanowires stand over the anode, ITO, with a thin inter-layer (10 nm to 15 nm) of TiO. The length of the CuPc nanowires can be varied by varying the length of the alumina template itself. CuPc nanowire lengths of 500 nm to 1 μm were investigated. Alumina acts as a wall separating nanowires from each other. The PEDOT:PSS acts as anode buffer layer. It is a thin and transparent film (100 nm – 200 nm) and can be spin-coated. It smoothens the surface of ITO anode [26], enhances adhesion to CuPc, and decreases hole injection barrier due to its relatively higher work function (5.1 ± 0.1 eV) on ITO and eventually improves the device performance.

CuPc, which acts like a p-type semiconductor, has a work function of about 5.3 eV with an energy gap of 1.7 eV. On the other hand aluminum has a work function of about 4.06 eV. As the work function of the metal is less than that of the semiconductor ($\Phi_m < \Phi_s$), which is of p-type, they form a Schottky contact. Figure 11 shows the energy level diagram for CuPc-Al Schottky junction. The difference in the work function provides an electric field at the CuPc-Al interface. This electric field is sufficient to break up the photogenerated excitons. Absorbed photons generate excitons that diffuse towards cathode or anode contact where they may dissociate to yield charge pairs or may recombine. Only the layer of organic material, which lies within an exciton diffusion length of a contact, can contribute to the photocurrent. Since exciton diffusion lengths are typically 1-10 nm, exciton diffusion limits charge carrier generation.

.

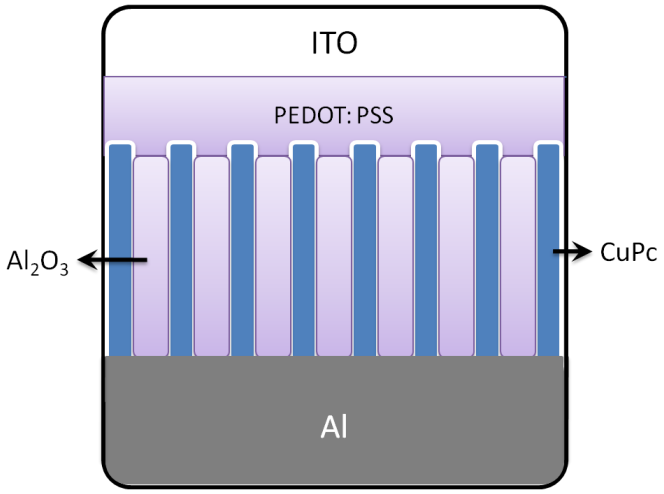

Figure 9: Device Structure Type-I; CuPc-Al forms a Schottky contact; CuPc ITO forms an ohmic contact

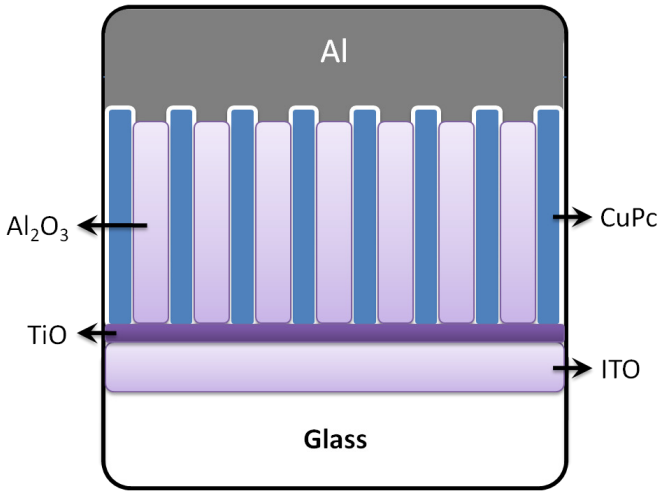

Figure 10: Device Structure Type-II; CuPc-Al forms a Schottky contact; CuPc-ITO forms an ohmic contact

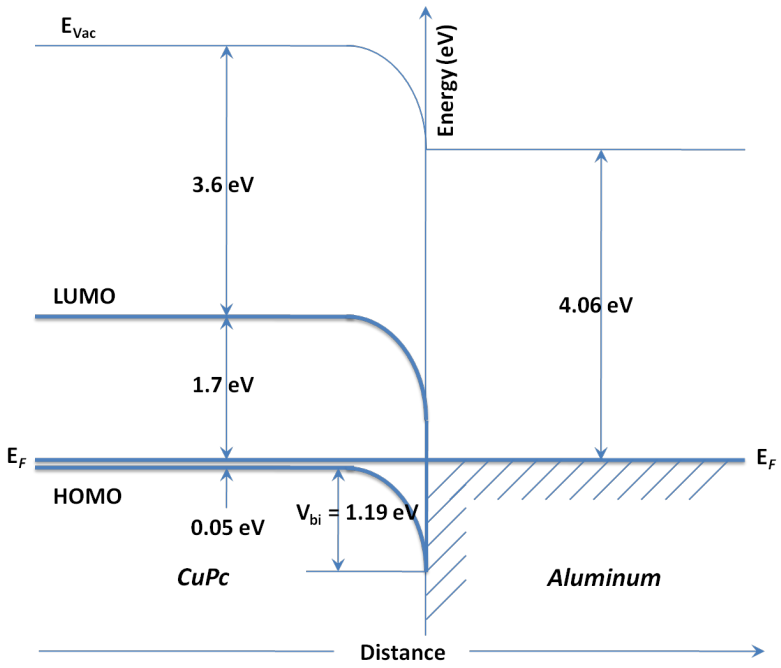

Figure 11: Energy level diagram of CuPc-Al junction

3. Experimental Procedure

The device structure of Type-I was fabricated by first preparing Anodized Aluminum Oxide (AAO) over Aluminum tape, filling it with CuPc by electrodeposition, spin-coating PEDOT:PSS and finally sputtering ITO. Type-II devices were fabricated by preparing AAO over ITO-glass, filling it with CuPc by electrodeposition and finally evaporating Aluminum.

3.1 Fabrication of nanoporous alumina over Aluminum tape

The nanoporous AAO templates were prepared by anodizing aluminum tape at room temperature, in a vertical two-electrode cell with platinum as a counter electrode. The electrolyte was a solution containing 0.3 M oxalic acid dissolved in de-ionized water; one side of the tape being protected by glue and paper. The 2-step anodization process, reported by S. Phok *et al* [20], was used in order to obtain highly ordered patterned pores. As the removal of the aluminum oxide barrier layer is critical for DC electrodeposition, a ramp down voltage was used for the removal of the barrier layer. This resulted in branching and reduced pore diameter at the bottom.

3.2 Fabrication of nanoporous alumina using ITO-glass templates

Glass substrates pre-coated with 150 nm thick conductive, transparent ITO anode were purchased from Delta Technologies. They were 1”x 2” in size with a sheet resistance of 4-8

Ω/square. These templates were sonicated using an ultrasonic bath in acetone for 2 minutes. Then, they were rinsed with isopropyl alcohol (IPA) and finally sonicated in distilled water. The cleaned samples were dried in Nitrogen. The ITO side of the templates was identified with the help of a multimeter by measuring the resistance. Using Torr International E-Beam Evaporator, a thin layer (10 nm to 15 nm) of Titanium (Ti) was vacuum evaporated at a chamber pressure of ~5.0E-6 torr. The templates were then annealed at 200^{o}C in air. Annealing oxidizes Ti to form TiO which acts as a good adhesion layer between Aluminum and ITO. Aluminum was then vacuum evaporated using E-Beam Evaporation with a thickness varying from 500 nm to 1 μm depending on the thickness of the alumina template required. The 2-step anodization process was then carried out as described above followed by a thermal treatment at 200^{o}C in air for several hours.

3.3 Electrodeposition of CuPc in AAO template

CuPc was electrodeposited inside the pores of alumina template supported by the underlying aluminum substrate. Pores were 500 nm to 1 μm in length and 20 nm to 30 nm in diameter. The electrolyte was a 50 ml chloroform ($CHCl_3$) solution containing 0.005 grams of CuPc with 1 ml Trifluoroacetic acid (CF_3COOH); CF_3COOH acted as a protonating reagent [19]. Using a Fisher Scientific weighing balance, 5 mg of CuPc was weighed into an 80 ml standard beaker. In order to improve the dissolution of CuPc, a small amount of $CHCl_3$ was added to the beaker and stirred before adding CF_3COOH. The beaker was then filled to 50 ml with $CHCl_3$ and stirred thoroughly. A 1"x1" platinum electrode was used as anode and the AAO template served as cathode. Electrodeposition was carried out with an applied DC voltage of 15V - 30V (ramped at the rate of 1V/min). During this electrodeposition step, a thin layer of CuPc (10nm – 50nm) also got deposited over the surface of aluminum oxide; N-N-Dimethylformamide solution was used for removing this top layer of CuPc. This process was repeated, typically two or three times, until the pores were completely filled with CuPc. The electrodeposited AAO templates were then annealed at 300^{o}C in vacuum for 5 hours and allowed to cool to room temperature.

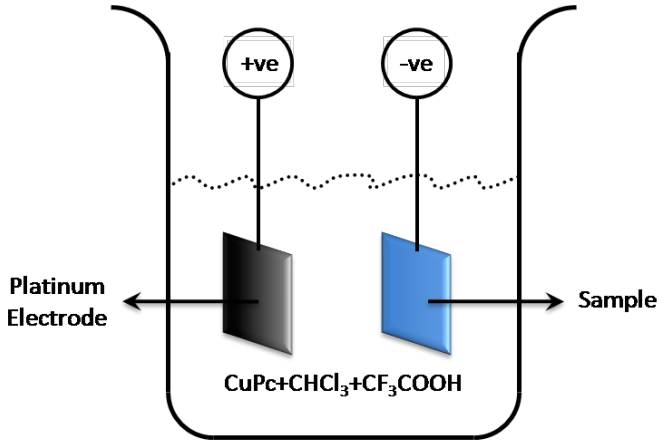

Figure 12: Electrodeposition setup

3.4 Spin Coating of PEDOT:PSS

One of the simplest and most common techniques of depositing thin films onto flat substrates is the technique of spin coating. The material to be deposited must be dissolved or dispersed into a solvent of some kind and this solution is then deposited onto the surface and spun-off to leave a uniform layer for subsequent processing stages**.**

For Type-I devices, after thermal treatment, PEDOT:PSS, purchased from Aldrich, was spin coated using Chemat Technologies spin coater. The spin coating was carried out at 4000 RPM for 40 seconds. The spin coated samples were then annealed in vacuum at 100^{o}C for 60 minutes. Annealing removes the excess water molecules in the PEDOT:PSS layer on the sample and also increases the adhesion between the PEDOT:PSS and CuPc. The samples were then allowed to cool down to room temperature.

3.5 Sputtering of ITO

Sputtering is a deposition process which physically removes a target material and deposits a firmly bonded coating onto the sample. The sputtering process occurs by bombarding the surface of the target material with gaseous ions (normally Ar+) using an RF power source. As these ions collide with the target, atoms or occasionally entire molecules of the target material are ejected and propelled against the sample, where they form a very tight bond. The resulting coating is held firmly to the surface by mechanical forces. When compared to evaporation, sputtering can get better uniformity over a large size. But, certain sputtering systems may require a medium level vacuum that can increase contamination.

The anode electrode, ITO, was sputtered using Hummer single target sputtering system. The spin-coated samples were masked with an aluminum foil having circular openings of about 0.07 cm^2 in area, to define the ITO sputtering areas. The Sputtering was carried out at 0.01 mTorr with Argon as the gas medium. The density, Z-factor and the thickness of ITO to be sputtered were pre-programmed in the system. 80 nm of ITO was sputtered at an average rate of 2 A^o/sec. The ITO sputtered makes a conducting contact with CuPc nanowires. This is the final step where we have the required device Al/CuPc/PEDOT:PSS and (or) ITO ready for characterization.

3.6 E-Beam Evaporation of ITO and Aluminum

A Torr International E-Beam Evaporator was used to evaporate ITO and Al for the fabrication of Type-II devices. The substrate is placed inside a vacuum chamber, in which a source of the material to be deposited is placed in a graphite crucible. An electron beam (E-beam) is aimed at the source material causing local heating. The source material is heated to the point where it starts to boil and evaporate. The vacuum is required to allow the molecules to evaporate freely in the chamber, and they subsequently condense on all surfaces.

Material characterization of the CuPc nanowires fabricated was performed with the techniques of X-Ray diffraction (Bruker-AXS D8 DISCOVER Diffractometer), optical absorption spectroscopy and scanning electron microscopy (Hitachi S-900 field emission SEM). Electrical characterization was performed with an automated system which included an *I-V* tester, a solar simulator and a HP 4192A LF impedance analyzer.

4. Results and Discussion

4.1 Characterization of CuPc using Scanning Electron Microscopy (SEM)

Figure 13 shows the scanning electron micrographs of a typical starting alumina templates used for electrodeposition of CuPc.

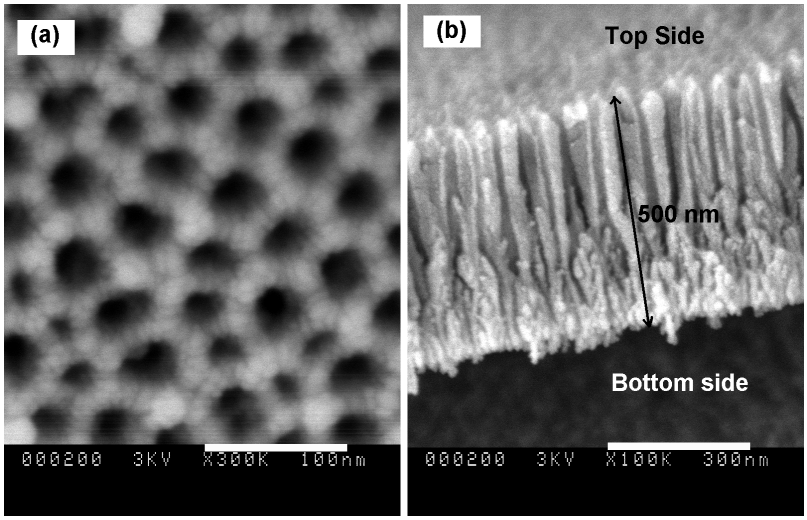

Figure 13: SEM micrographs: (a) top view and (b) cross section of a typical 0.5 μm thick AAO/Al template anodized at 20V followed by 25V

The top view of the template (Figure 13(a)) reveals hexagonal packed pores with pore diameter in the 20 nm to 30 nm range and pore spacing in the 30 nm to 40 nm range, for a template anodized at 25V at room temperature. The cross-sectional view of this 0.5 μm long AAO/Al template is shown in Figure 13(b). It can be seen that the pores get narrower along the bottom with branching as a result of ramp down voltage. The pore diameters at the bottom of the anodized AAO/Al template ranged from 15 nm to 20 nm.

The X-ray diffraction pattern of AAO/Al revealed that the AAO template was amorphous. Cross sectional view of the AAO sample after electrodeposition, with CuPc filling the pores from top to bottom is seen in Figure 14(a). The left side of the image includes the top surface of the AAO template with the pore openings. Figure 14(b) shows the cross section at another location near the bottom (Al-Al_2O_3 interface) of the AAO pores. The unfilled portions of AAO pores seen in Figure 14(b) are thought to have lost their CuPc nanowires due to the stress produced during the process of breaking the device and mounting it on the stub for electron microscopy.

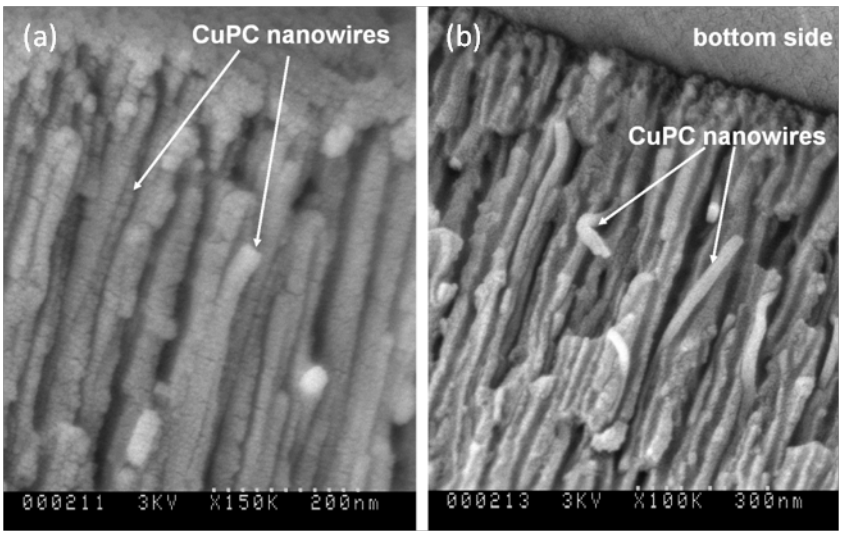

Figure 14: Scanning electron micrographs of CuPc nanowires electrodeposited in AAO/Al template at room Temperature; cross sectional views at, (a) a location near the top, (b) a location near the bottom of the pores

In the electrolyte solution, CuPc forms complex structures of the form CuPc $(nH)^{n+}$ (n varying from 1 – 4) in the presence of excess CF_3COOH [19]. These complexes, having a net positive charge, migrate towards the cathodic alumina substrate. In the experiments, it was observed that the CuPc nanowires grow not only from the bottom of the pore but also from the walls. This can be attributed to the presence of an electric field not only at the bottom of the pore but also on the inner side of the walls of the pore. This electric field is made possible by the presence of the un-oxidized, metallic aluminum at the central core of the alumina walls, which is in contact with the bottom aluminum substrate.

4.2 Optical Absorption

Measurement of the optical absorption spectrum of CuPc nanowires grown on aluminum tape (Type-I) was complicated by the presence of the opaque aluminum substrate. Therefore, Type-II devices were used for optical absorption measurements. CuPc has two absorption bands; Sorret band (S-band) in the UV-region and Q-band in the visible region. The S-band is related to the direct electronic transition from d-π^* orbitals. The absorption peaks in the visible region (Q-band) are generally interpreted in terms of π-π^* excitation between bonding and anti-bonding molecular orbitals [23].

Figures 15-16 show the optical absorption curves for various lengths of CuPc nanowires annealed at 200^{o}C and 300^{o}C.

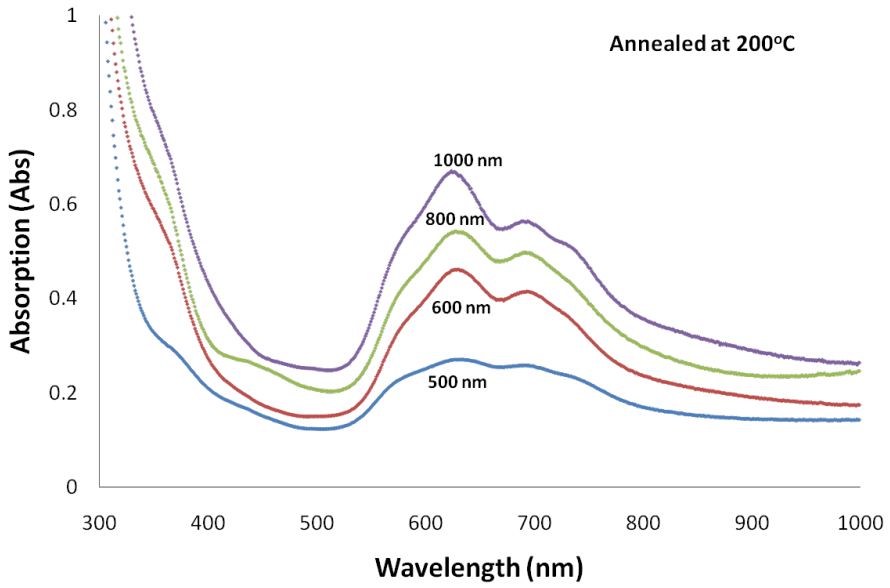

Figure 15: Optical absorption of CuPc nanowires for different nanowire lengths varying from 500nm to 1000nm annealed at 200°C

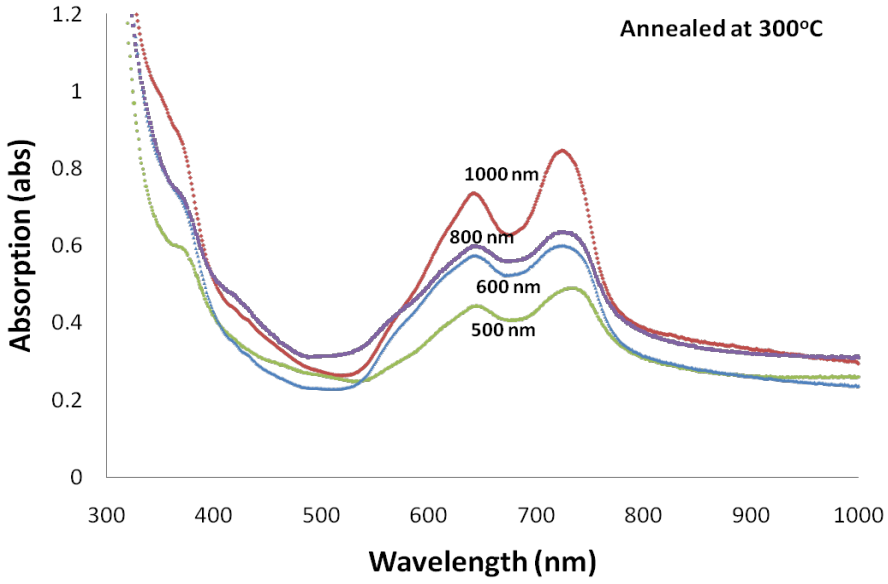

Figure 16: Optical absorption of CuPc nanowires for different nanowire lengths varying from 500nm to 1000nm annealed at 300°C

CuPc nanowires annealed at 200°C having a preferred α-phase crystallization, (discussed in section 4.3) had absorption peaks at 620nm and 691nm corresponding to dimer and monomer peaks respectively. It can be seen from Figure 15 that the dimer phthalocyanine has higher

absorption when compared to monomer phthalocyanine. When annealed at 300°C, CuPc nanowires, having β-phase crystallization, had absorption peaks at 644 nm and 724 nm as shown in Figure 16. Also, the peak at longer wavelength (724 nm) has higher absorption value. This could be attributed to the fact that β-CuPc has higher absorption at longer wavelengths when compared to that of α-CuPc [15].

An important observation was that with pulse voltage CuPc deposits as a film but does not go into the pores while with DC ramp voltage CuPc fills the pores. To illustrate this, CuPc was deposited in AAO templates over ITO glass using pulsed voltage in one case and a D.C. ramp voltage in another case. The optical absorption results are shown in Figure 17.

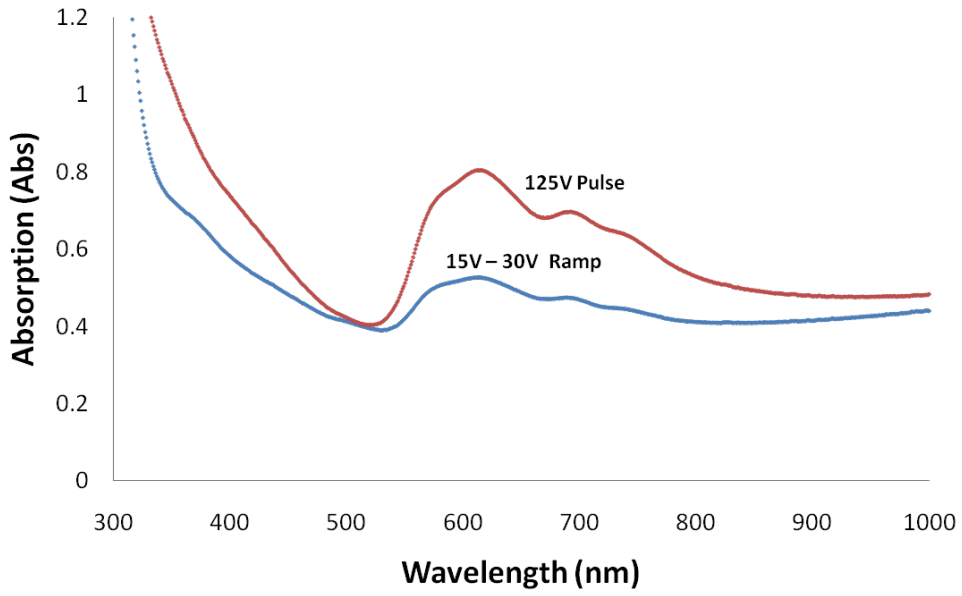

Figure 17: Optical absorption spectra of electrodeposited CuPc nanowires embedded in an AAO template on a glass-ITO substrate

For the top curve, the electrolyte was a 150 ml chloroform ($CHCl_3$) solution containing 0.004g of CuPc and 5 ml of Trifluoroacetic acid (CF_3COOH); electrodeposition was conducted for four minutes, with voltage pulses of 125V amplitude, 2 seconds pulse width and 6 seconds time period. The top CuPc layer was not removed intentionally. For the bottom curve, the electrolyte was a 50 ml chloroform solution containing 0.005 grams of CuPc with 1 ml Trifluoroacetic acid; electrodeposition was conducted with a D.C. voltage ramped from 15-30 V at a rate of 1V/min with the top layer removed. Both devices were annealed at 200°C. The SEM micrograph of the pulse deposited CuPc showed a thick CuPc film over the top (~700nm) but no

deposition inside the pores (Figure 18a) while with D.C. voltage CuPc filled the pores forming nanowires (~500nm) (Figure 18(b)). Thus, we note that a D.C ramp voltage is preferable for getting the CuPc into the pores of AAO.

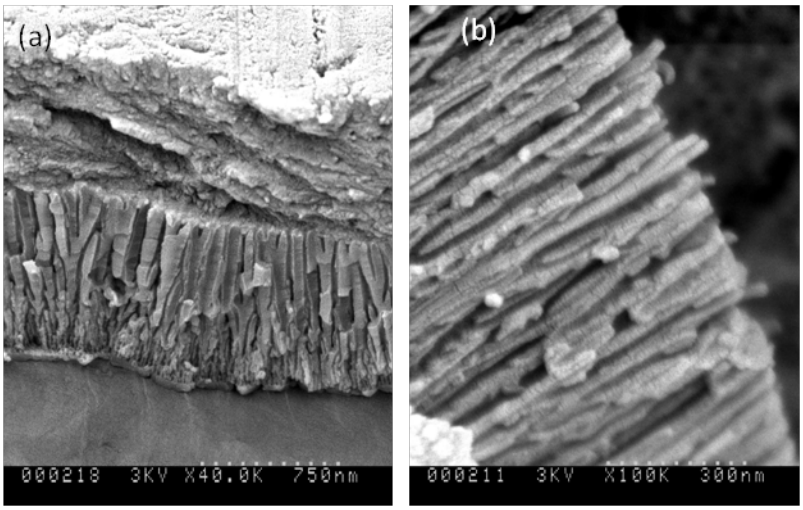

Figure 18: Scanning electron micrographs of CuPc electrodeposited in AAO template on a glass-ITO substrate using (a) 120V/0V pulse voltage and (b) 15V-30V D.C ramp voltage

The absorption curves for both conditions show peaks at 620 nm and 691 nm. The film deposited with 125V pulse showed greater absorption than the nanowires deposited with D.C. ramp voltage. This could be attributed to the fact that CuPc film formed over alumina (Figure 18(a)) has a greater quantity of CuPc when compared to CuPc nanowires inside the pores (Figure 18(b)), as nearly 50% of the volume is occupied by alumina in the later case. As alumina is transparent to visible light, the alumina part of the device does not contribute to absorption. Also the film formed (700nm) is thicker than the nanowire length (500nm).

4.3 X-Ray Diffraction Characteristics

It is well known that CuPc has three dominant crystal phases: α-, β- and χ-phases [25]. Figures 19-20 show the X-ray diffraction pattern of CuPc nanowires electrodeposited into the AAO and subjected to post deposition annealing treatments. Annealing was carried out for 5 hours in vacuum ambient in each case. The X-ray diffraction pattern of the as-deposited nanowires (Figure 19(a), (AD)), those annealed at 100^{o}C (Figure 19(b)), and those annealed at 200^{o}C (Figure 20(a)), show the dominance of α–phase. When annealed at 300^{o}C, β–phase becomes dominant (Figure 20(b) [17, 26-27]). The peaks at 2θ values of 6.8^{o} and 7.02^{o} correspond to α (001) and β (100)

respectively. In Figures 19-20, the XRD peaks of ITO at 2θ values of 21.3°, 30º, 35º, 51º and 60º and alumina peak at 45° are also observed.

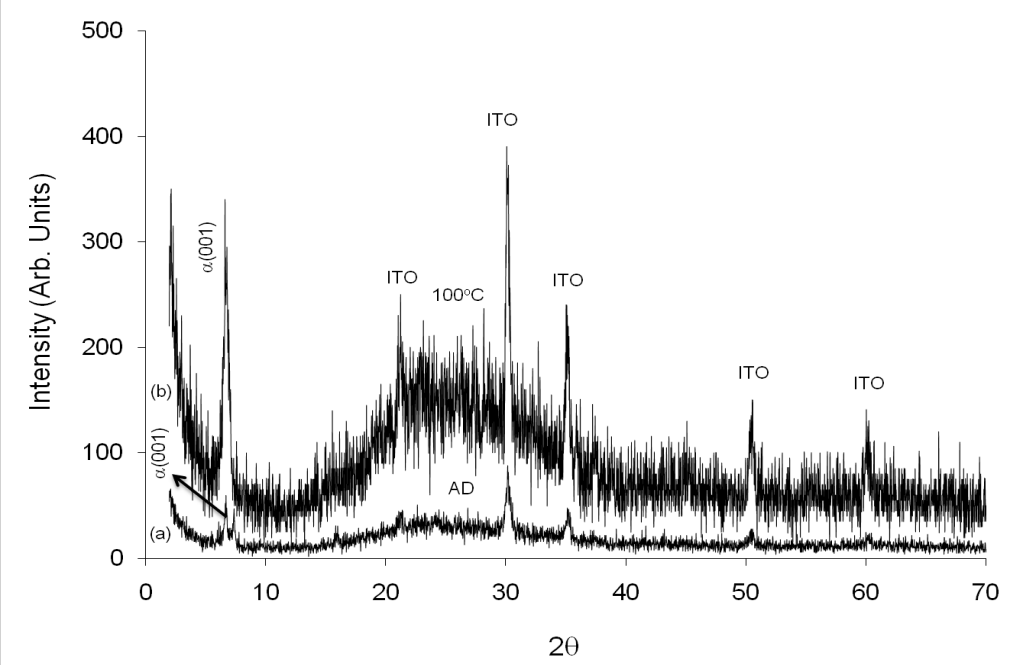

Figure 19: X-ray Diffraction pattern of electrodeposited CuPc nanowires in AAO template on a glass-ITO substrate (a) as-deposited (AD), (b) annealed at 100°C (plot (b) scaled for clarity)

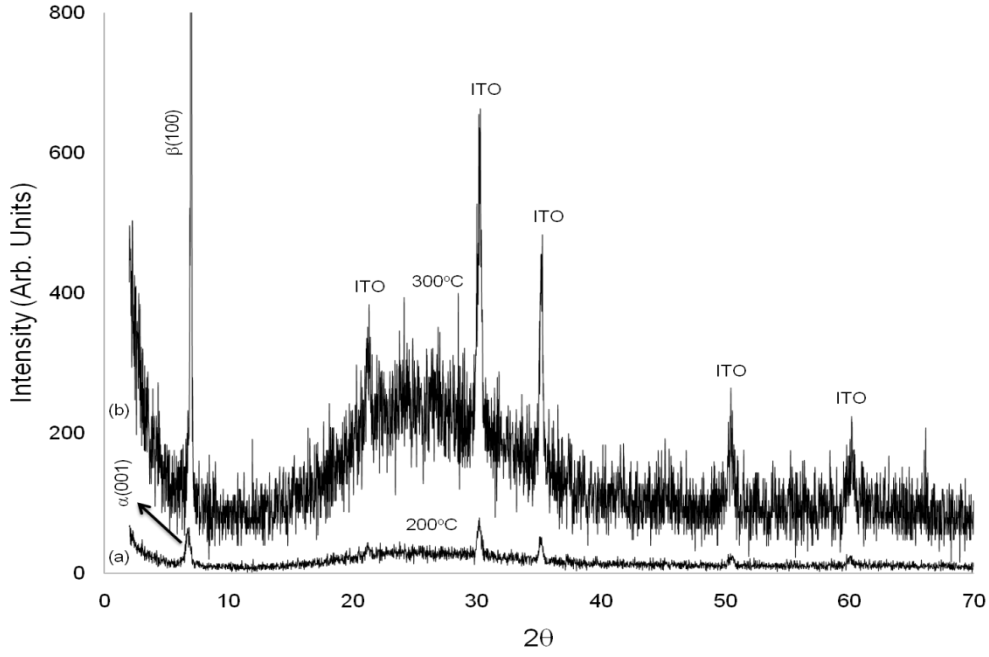

Figure 20: X-ray Diffraction pattern of electrodeposited CuPc nanowires in AAO template on a glass-ITO substrate: (a) annealed at 200°C, (b) annealed at 300°C (plot (b) scaled for clarity)

4.4 Schottky Diode Characteristics

The current density (J) vs voltage (V) characteristics of Type-I and Type-II devices for various thicknesses of CuPc are shown below. The J-V characteristics were also measured under illumination to see if the devices exhibit photovoltaic effect. Figures 21-24 show the J-V characteristics of CuPc-Al Schottky diodes for varying lengths of CuPc nanowires over Al-tape. Figure 25 and Figure 26 show the dark and the light curves for various CuPc nanowire lengths respectively. Similarly, Figures 27-32 show the corresponding J-V characteristics of Type-II devices.

It can be seen that for all the devices current is higher under illumination when compared to their corresponding dark currents owing to the photoconductance of CuPc. Also, as the length of the CuPc nanowires increase, the currents decrease due to the increased internal resistance of the device.

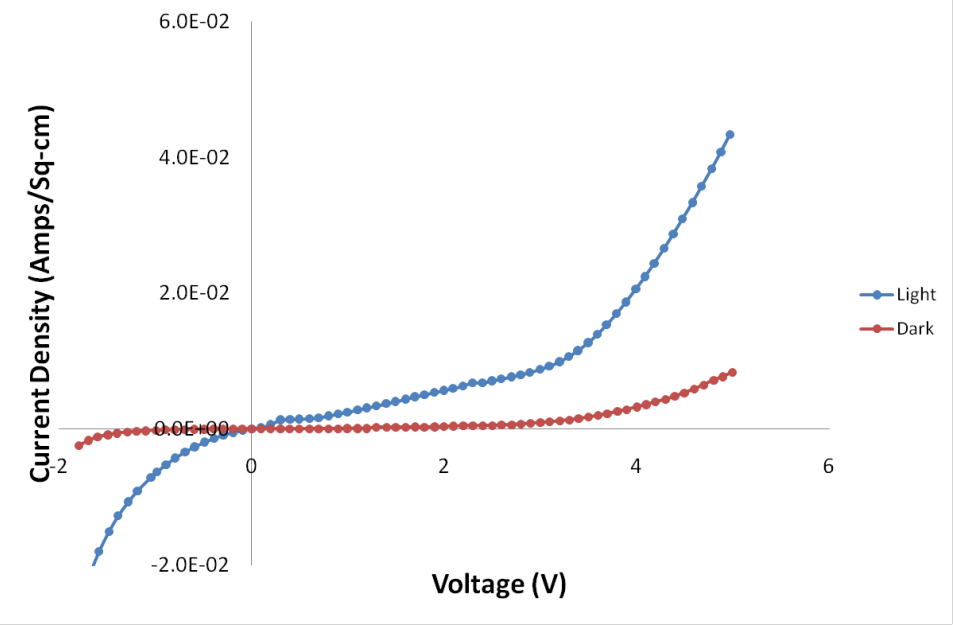

Figure 21: J-V characteristics of a CuPc-Al Schottky diode with 500 nm long CuPc nanowires over Al-tape (Type-I)

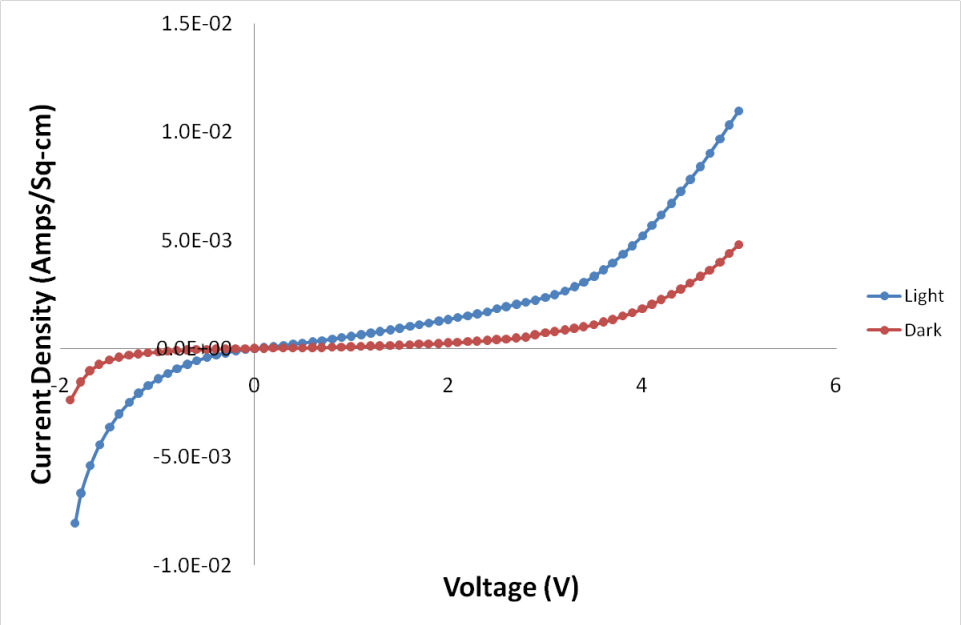

Figure 22: *J-V* characteristics of a CuPc-Al Schottky diode with 600 nm long CuPc nanowires over Al-tape

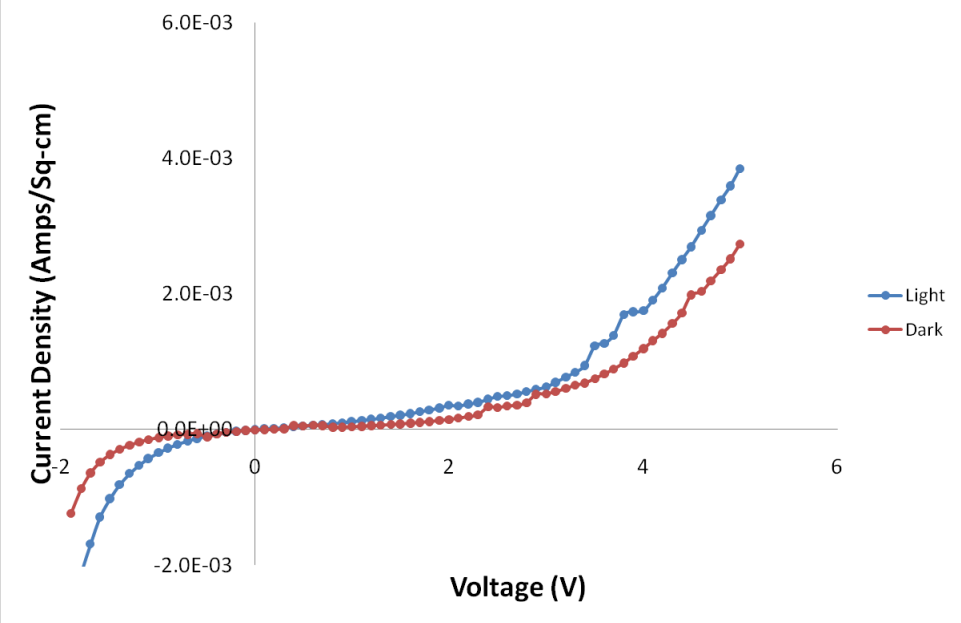

Figure 23: *J-V* characteristics of a CuPc-Al Schottky diode with 800 nm long CuPc nanowires over Al-tape

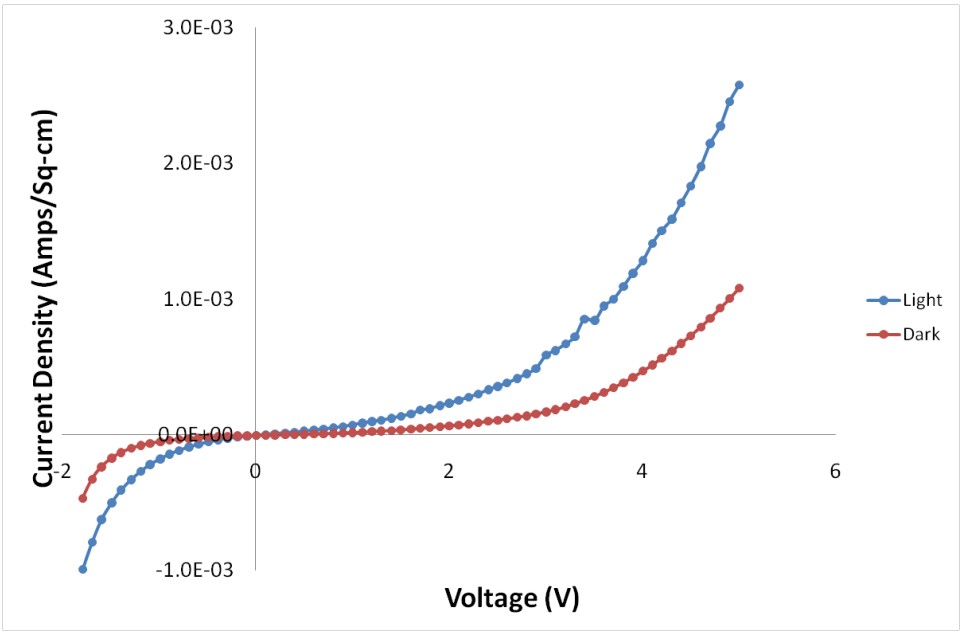

Figure 24: *J-V* characteristics of a CuPc-Al Schottky diode with 1000 nm long CuPc nanowires over Al-tape

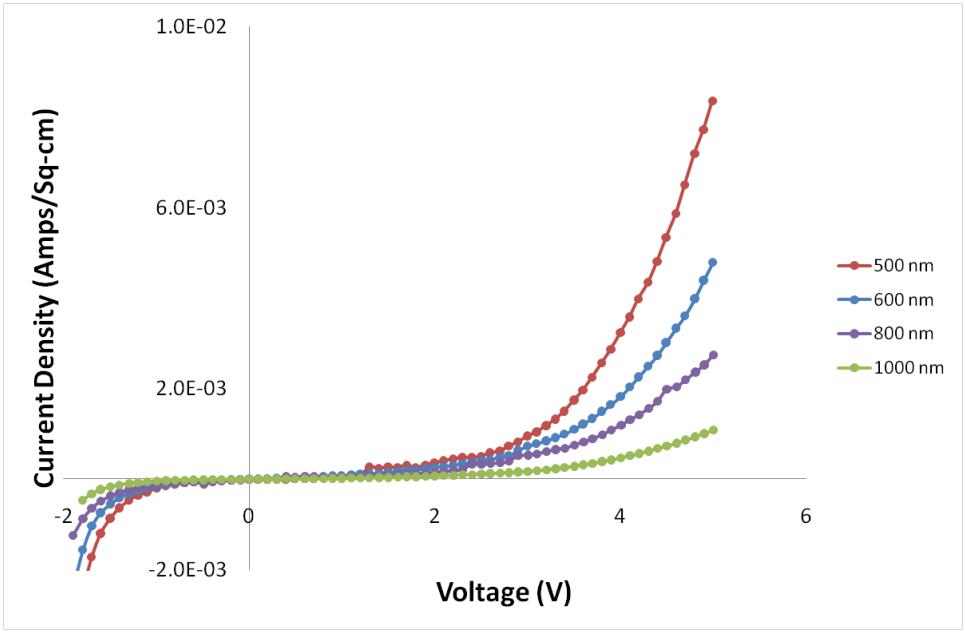

Figure 25: *J-V* characteristics of a CuPc-Al Schottky diode in Dark over Al-tape (Type-I); comparing different thicknesses

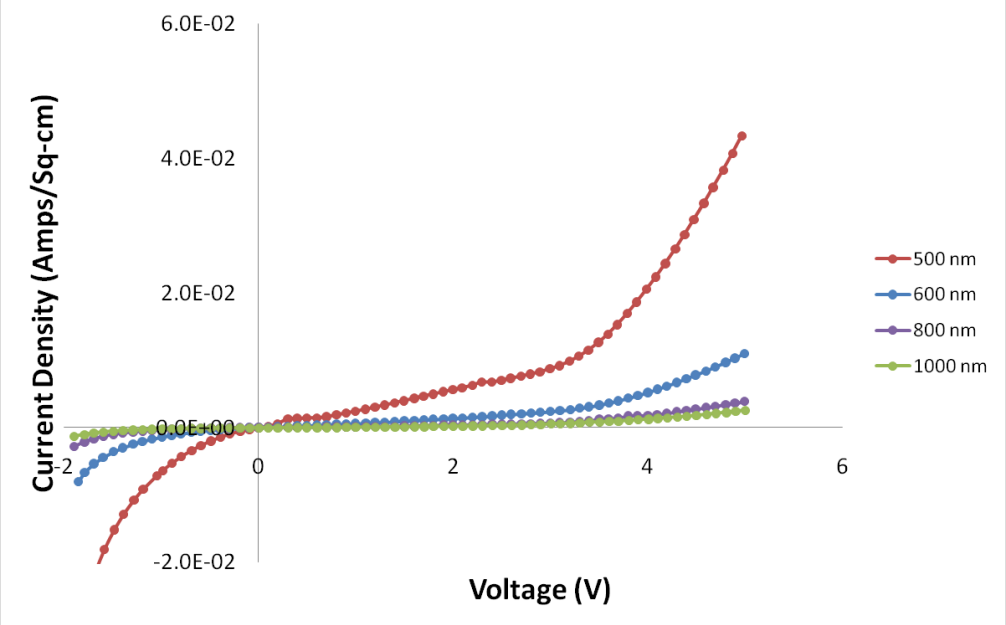

Figure 26: *J-V* characteristics of a CuPc-Al Schottky diode in Light over Al-tape (Type-I); comparing different thicknesses

Photoconductance was exhibited by all the devices but no photo voltaic effect was observed. The explanations are discussed later in detail. Diode analysis was performed for these devices and the values of the effective reverse saturation current (J_o) and the effective diode ideality factor (η) were calculated to fit the equation,

$$J = J_0[e^{\left(\frac{qV}{\eta kT}\right)} - 1] \ldots\ldots (1)$$

The results are tabulated in Tables 1-2.

Table 1: Diode parameters for the CuPc-Al Schottky diodes in Dark over Al-tape (Type-I)

Nanowire Length	Series resistance (R_s) (Ohms)	Effective J_o (μA/cm^2)	Diode Ideality Factor (η)
500nm	152	10.1	26.5
600nm	247	13.8	27
800nm	450	10	27.2
1000nm	1274	4.1	27.9

Table 2: Diode parameters for the CuPc-Al Schottky diodes in Light over Al-tape (Type-I)

Nanowire Length	Series resistance (R_s) (Ohms)	Effective J_o (μA/cm^2)	Diode Ideality Factor (η)
500nm	37	938.3	23.3
600nm	149	139.5	27.7
800nm	381	19.9	33
1000nm	799	10.6	39.8

The *J-V* characteristics of Type-II devices for various thicknesses of CuPc are shown below.

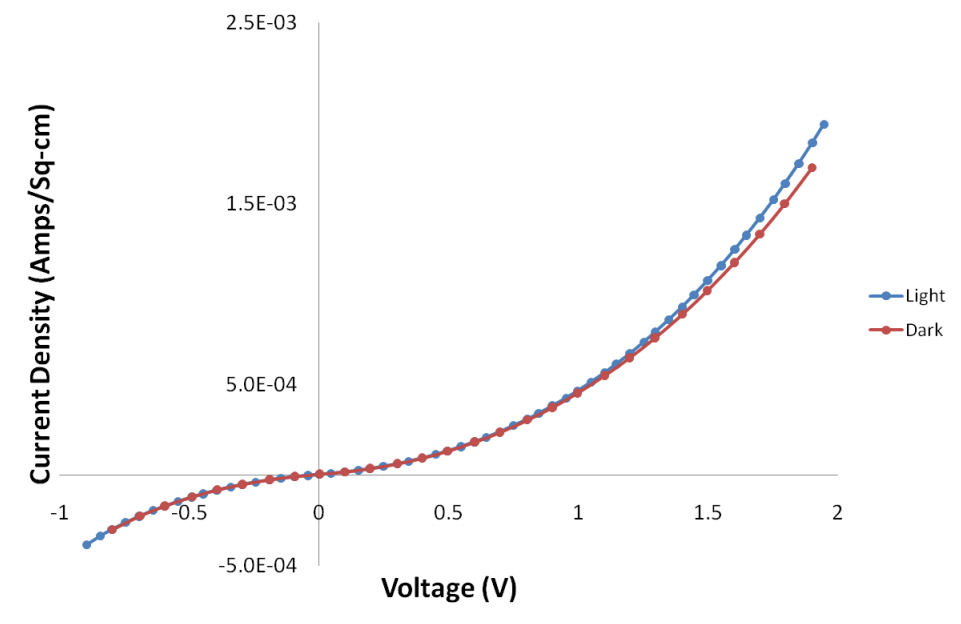

Figure 27: *J-V* characteristics of a CuPc-Al Schottky diode with 500 nm long CuPc nanowires over ITO-glass (Type-II) templates

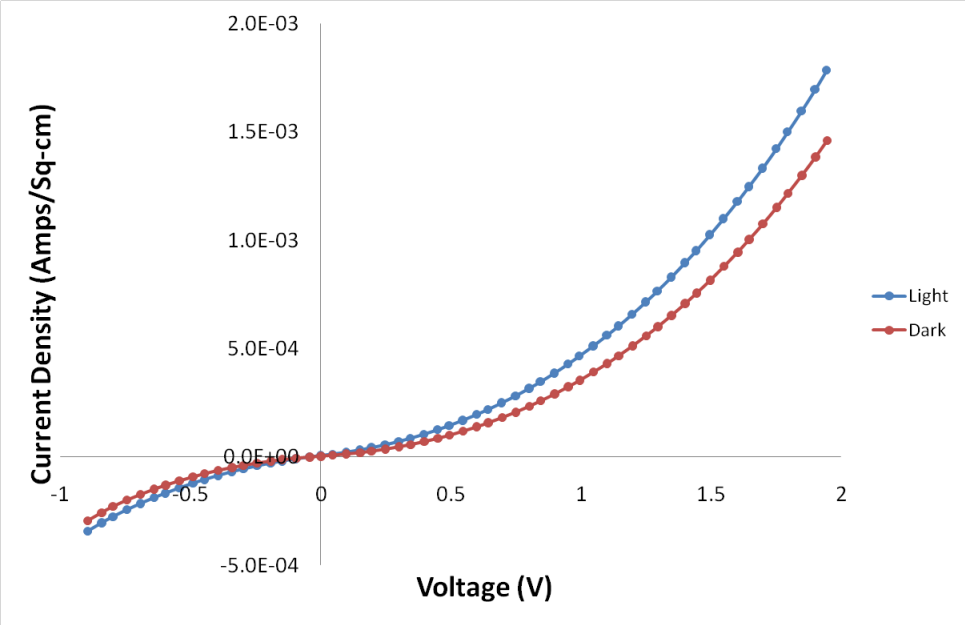

Figure 28: *J-V* characteristics of a CuPc-Al Schottky diode with 600 nm long CuPc nanowires over ITO-glass templates

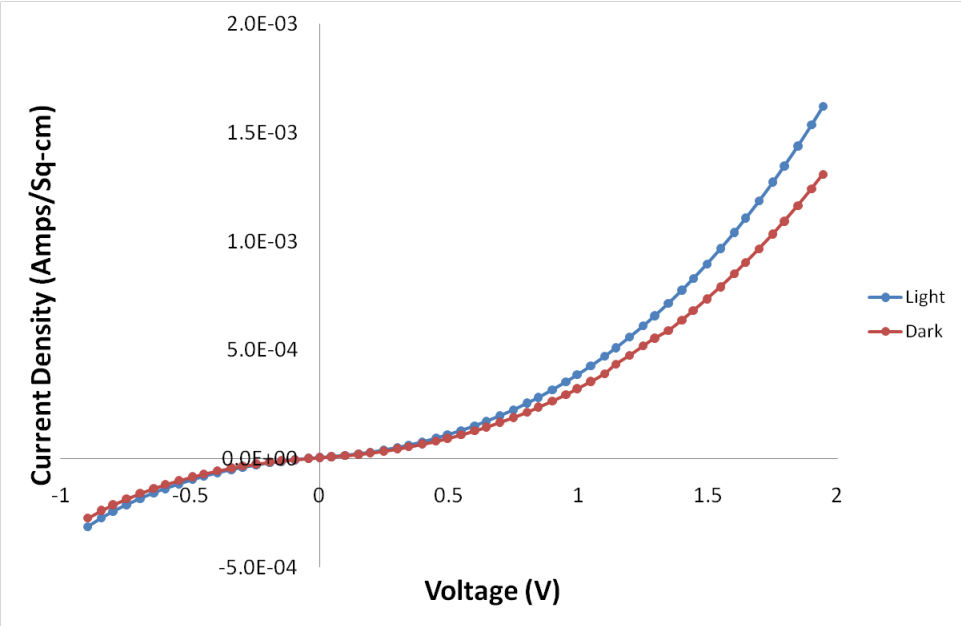

Figure 29: *J-V* characteristics of a CuPc-Al Schottky diode with 800 nm long CuPc nanowires over ITO-glass templates

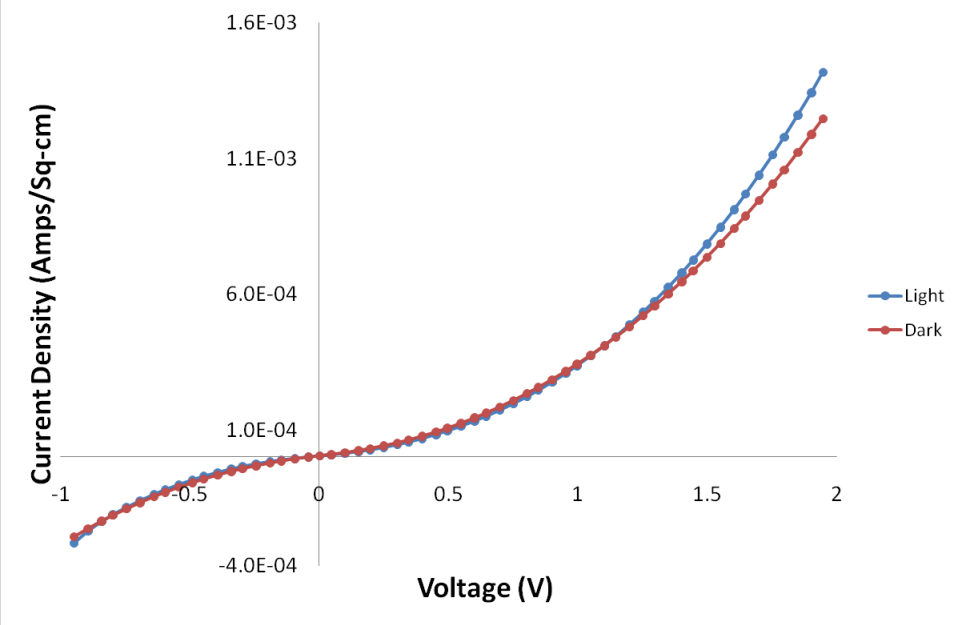

Figure 30: *J-V* characteristics of a CuPc-Al Schottky diode with 1000 nm long CuPc nanowires over ITO-glass templates

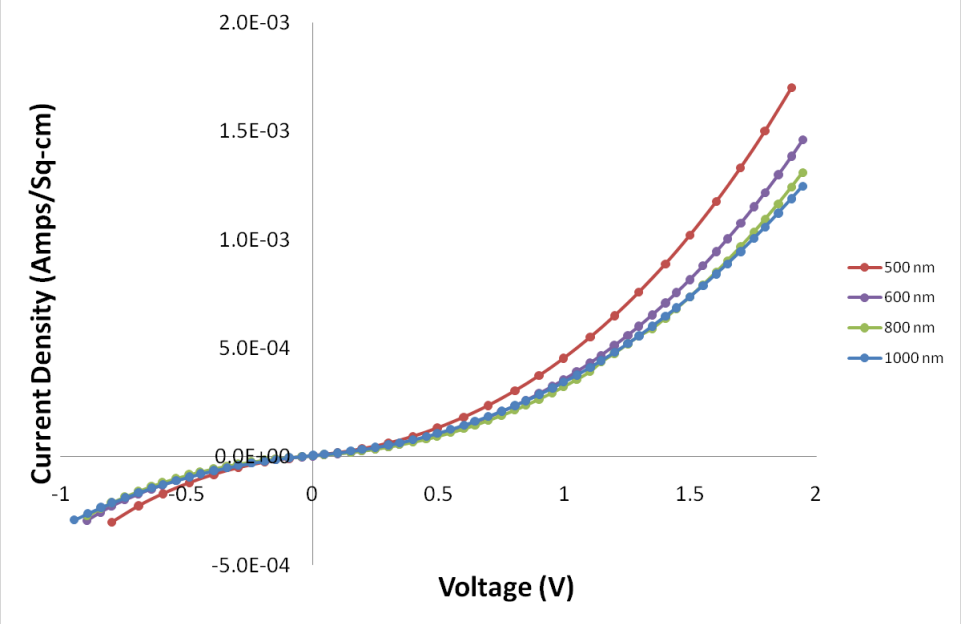

Figure 31: *J-V* characteristics of a CuPc-Al Schottky diode in Dark over ITO-glass (Type-II) templates; comparing different thicknesses

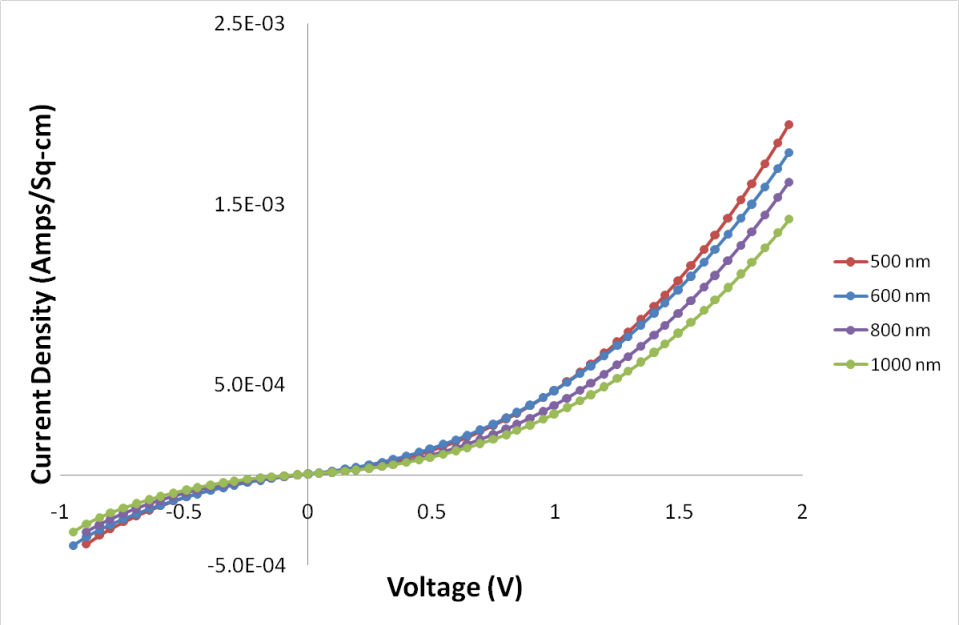

Figure 32: *J-V* characteristics of a CuPc-Al Schottky diode in Light over ITO-glass (Type-II) templates; comparing different thicknesses

Table 3: Diode parameters for the CuPc-Al Schottky diodes in Dark over ITO-glass (Type-II) templates

Nanowire Length	Series resistance (R_s) (Ohms)	Effective J_o (μA/cm^2)	Diode Ideality Factor (η)
500nm	528	17.5	8.9
600nm	586	13.4	9.3
800nm	660	12.8	9.3
1000nm	769	18.5	9.5

Table 4: Diode parameters for the CuPc-Al Schottky diodes in Light over ITO-glass (Type-II) templates

Nanowire Length	Series resistance (R_s) (Ohms)	Effective J_o (μA/cm^2)	Diode Ideality Factor (η)
500nm	433	15	8.9
600nm	498	18	9
800nm	521	12.2	9.2
1000nm	588	13.5	9.5

From the *J-V* analysis we can observe that as the length of the nanowires increase, the series resistance increases (R_s) and hence the current densities (J) decrease. Also, the diode ideality factor (η) increases with increase in nanowire length. It can also be observed that the current densities are higher under illumination.

Figure 33 shows the *J-V* characteristics of a Type-I Schottky diode with 500 nm long CuPc nanowires embedded in the 0.5 µm deep porous alumina template sitting on top of the un-anodized aluminum electrode. To study the effect of PEDOT: PSS buffer layer, a 100 nm thick PEDOT: PSS layer was introduced between the embedded CuPc nanowires and the ITO electrode; the device structure was thus modified to Al/CuPc/PEDOT:PSS/ITO. *J-V* characteristics of this device are shown in Figure 34. The diode parameters are calculated and are tabulated in Table 5. It is interesting to note that the measured value of effective diode ideality factor (η) is larger than 2.0.

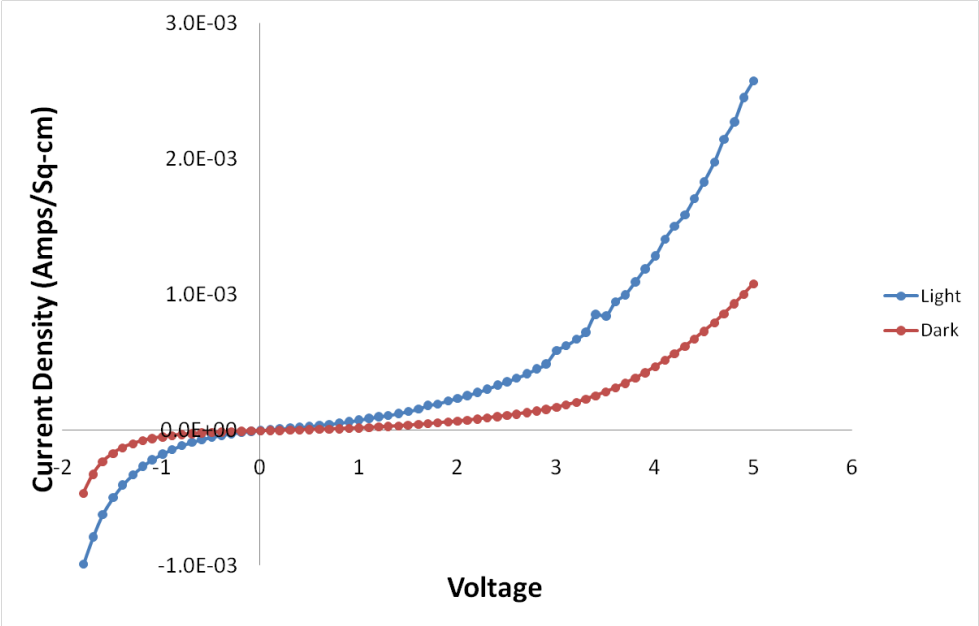

Figure 33: *J-V* characteristics of a CuPc-Al Schottky diode with 500 nm long CuPc nanowires

The buffer interlayer of PEDOT: PSS is known to improve the contact between CuPc and ITO [7, 31]. Comparing Figures 33 and 34, we see that, indeed higher currents and improved diode behavior is seen in Figure 34; series resistance in high forward bias is reduced by an order of magnitude. Also, in Figure 34, the sensitivity of the CuPc film and the CuPc-Al junction to the incident light is revealed. Not only is the current higher under illumination, but the lift-off voltage in the forward bias is also smaller. This indicates that, in addition to the effect of the

photoconductivity of the CuPc film, increase in current with illumination is related to the modification of the CuPc-Al junction interface by the incident light so that the junction barrier potential is reduced. The diode ideality factors are substantially different, 23.3 in the dark and 12.2 under illumination as shown in Table 5.

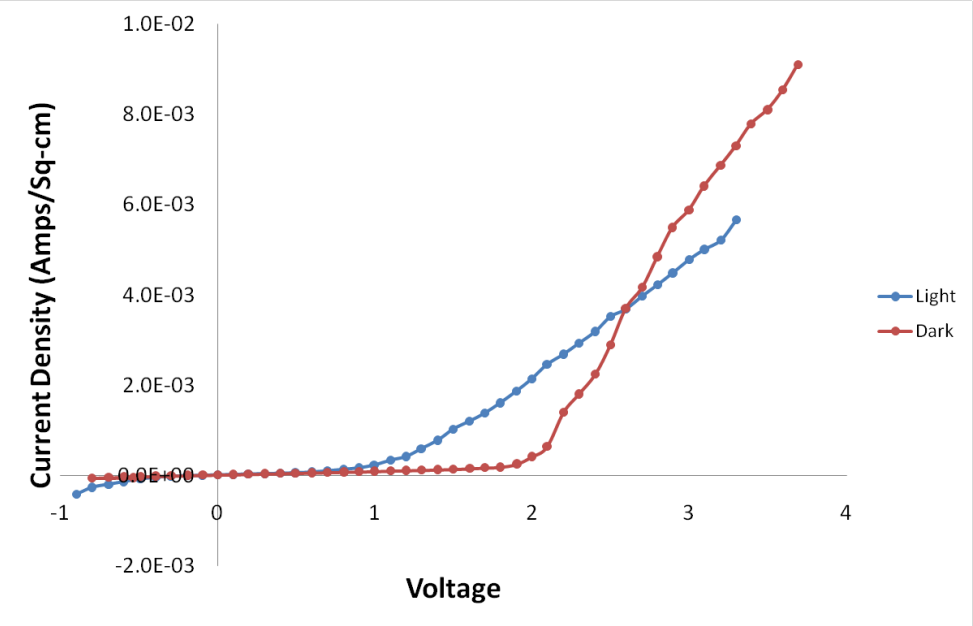

Figure 34: *I-V* characteristics of ITO-PEDOT: PSS-CuPc-Al Schottky diode with 500nm long CuPc nanowires

Table 5: Diode parameters for the ITO-CuPc-Al and ITO-PEDOT:PSS-CuPc-Al Schottky diodes on 500nm long CuPc nanowires embedded in a porous alumina template (Type-I)

Condition	Series resistance (R_s) (Ohms)	Effective J_o (μA/cm^2)	Effective Diode Ideality Factor (η)
Dark - Without PEDOT:PSS	1274	2.5	24.5
Light - Without PEDOT:PSS	799	1.0	23.3
Dark - With PEDOT:PSS	217	7.0	13.4
Light – With PEDOT:PSS	171	1.3	12.2

It is proposed that the interface states and traps near the junction between CuPc and Al play a dominant role in the current transport process in this device and these interface states and traps are altered when the Schottky diode is under illumination. Interface recombination currents would also help explain the large values of effective diode ideality factors [20].

Mechanism of current transport in an ITO/CuPc/Al device is not yet fully understood. Previous authors [23-24] have, in preliminary models, assumed that this device behaves in a manner similar to the Schottky diodes on inorganic semiconductors, where thermionic emission across the potential barrier at the metal-semiconductor junction plays a dominant role, leading to a current voltage of the form of equation (1), with η =1 [25]. In practice, values of J_o and η can vary widely, depending upon the actual mechanism of current transport in the device, in addition to or instead of the pure thermionic emission [22]. Values of η substantially higher than 1 have been reported in literature [23, 7], especially for Schottky diodes and heterojunctions, where interface states and traps abound, turning interface recombination and tunneling into major current flow processes.

Rajesh *et al* [21] and Jarosz [24] analyzed the reverse saturation current in thermally evaporated CuPc-Al and CuPc-Au Schottky diodes. Their results indicated that the Schottky-Richardson emission rather than the Poole-Frenkel emission was dominant. However, a value of η as high as 3.02 was reported in [21]. In this work also, we have found the value of η to be much larger than 1 for the electrodeposited CuPc. It seems very likely that, in addition to thermionic emission, charging and discharging of trap levels in CuPc, recombination of charge carriers, tunneling between aluminum and trap levels in CuPc and the lowering of the potential barrier at high electric fields may be playing a significant role in charge transport. These need to be considered in the modeling of the CuPc-Al device.

Gayatri previously reported a high V_{oc} of 1.19 V for CuPc-Al Schottky diodes over planar substrates [16]. The fact that photovoltaic response was observed in the Glass-ITO-PEDOT: PSS-CuPc (200nm)-Al Schottky diodes on planar glass substrate, but not in the Al-CuPc (500 nm)-PEDOT: PSS-ITO Schottky diodes on embedded CuPc nanowires could be attributed to the rather large CuPc thickness of 500 nm in the latter case. This is much larger than the exciton diffusion length of CuPc and therefore it is possible that no excitons are reaching the CuPc-Al junction in the nanowire case. Another probable reason could be the domination of interface recombination at the CuPc-alumina interface along the length of the CuPc nanowires. Also, the nature of the CuPc-on-aluminum junction may be substantially different than the nature of the

aluminum-on-CuPc junction, leading to variations in the defect, vacancy and trap densities in CuPc. Effective diode ideality factors (η), for these two Schottky diodes under illumination, are substantially different; and are tabulated in Table 2 and Table 4 respectively.

4.5 Low Temperature Characteristics

For comparison, low temperature *I-V* characteristics were measured for a commercially available IR 90SQ045 Schottky diode.

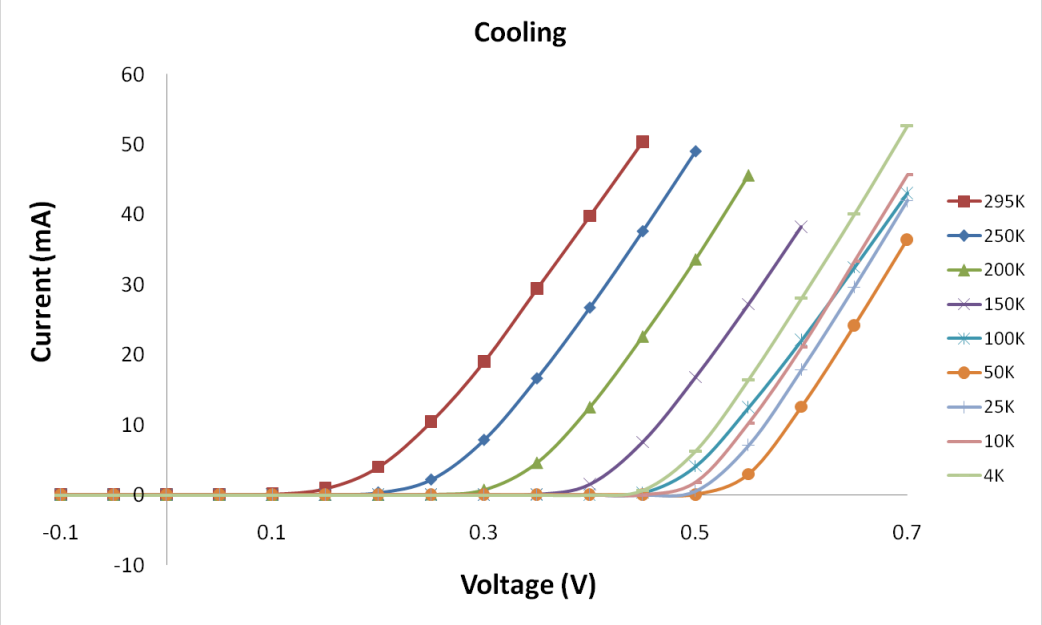

Figure 35: The Low Temperature *I-V* characteristics of IR 90SQ045 Schottky diode; cooling cycle

The *I-V* characteristics were measured in two cycles; cooling (from 295 K to 5 K) and heating (from 5 K to 295 K). Figures 35-40 show the I-V plots for heating and cooling cycles. A decrease in the currents for a given voltage was observed during the cooling cycle down to a temperature of 50 K. At temperatures below 50 K, an increase in the currents was observed. The characteristics can be understood by the thermionic emission theory and the diffusion processes. As the temperature is reduced from 295 K to 50 K, the diffusion of electrons and holes is slowed down as they don't have sufficient energy. As a result, the current decreases with decrease in the temperature. At 50 K the current due to the thermionic emission and diffusion processes is practically zero.

Below 50 K, the carriers start to freeze out and the ideality factor deviates from its original value and is a slowly varying function of temperature [17]. Also, the actual barrier height varies non-linearly with the bias [32] resulting in an increase in the diode ideality factor with decrease in temperature. Below 20 K the ideality factor varies more rapidly. The cooling and heating cycle plots are shown more clearly in Figures 36-37 and Figures 39-40 respectively.

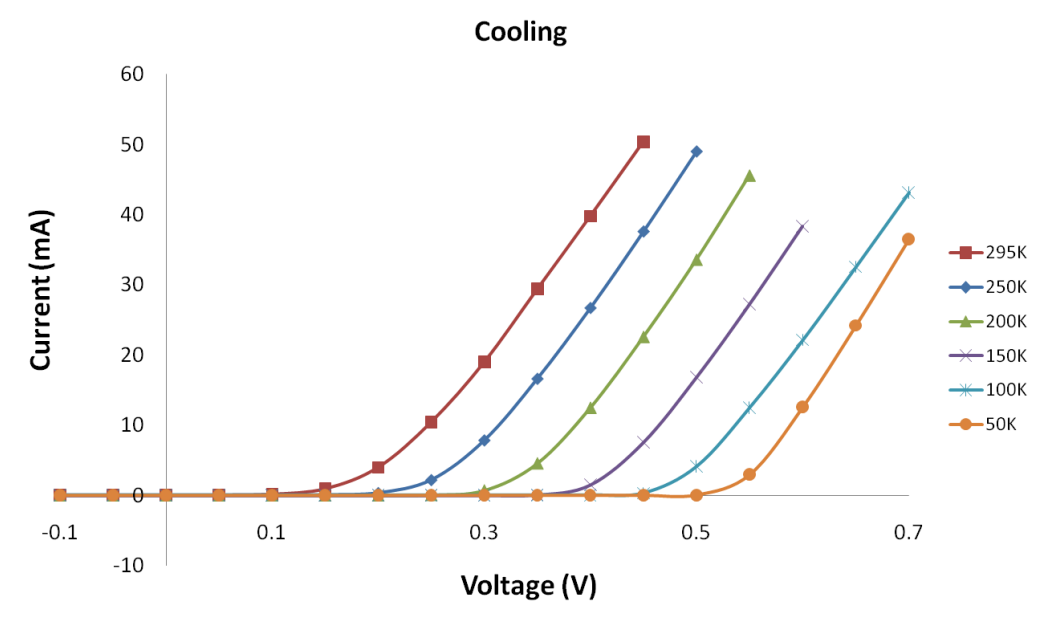

Figure 36: Figure 34 with temperatures from 295 K to 50 K

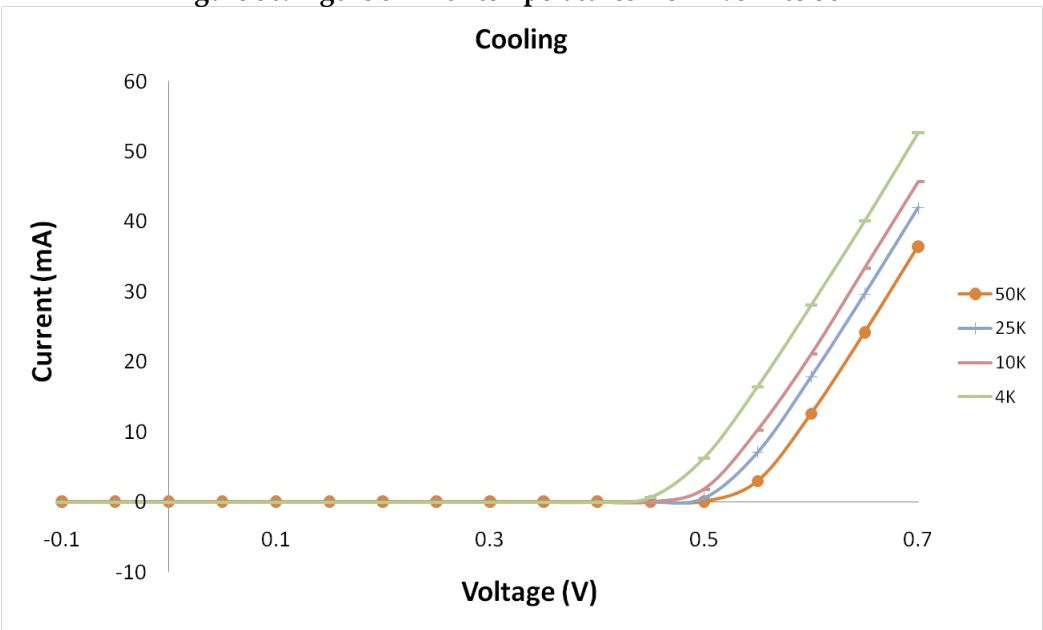

Figure 37: Figure 34 with temperatures from 50 K to 4 K

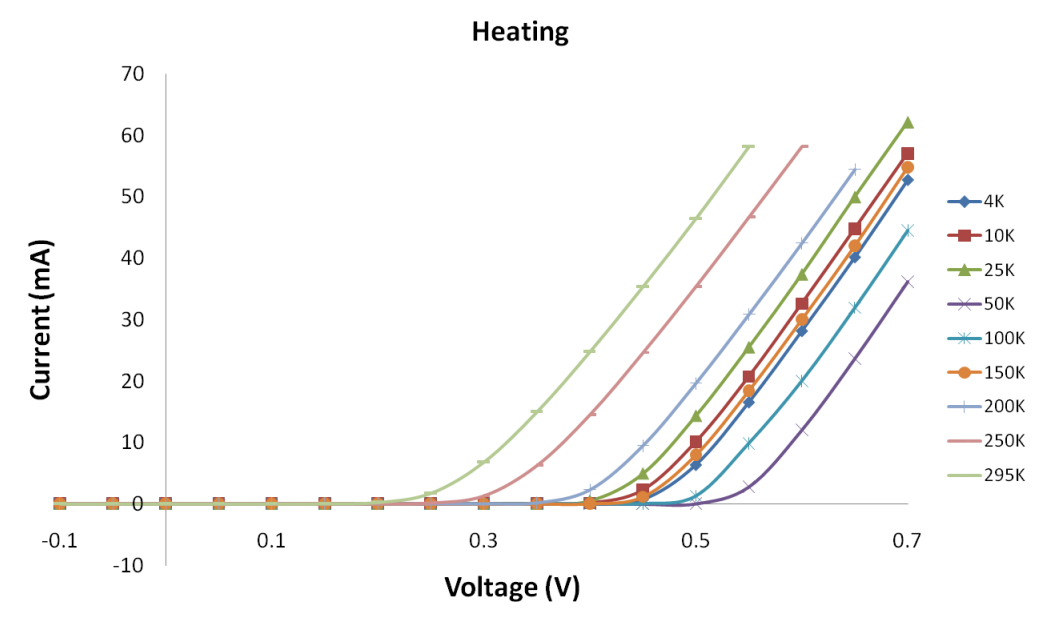

Figure 38: The Low Temperature I-V characteristics of IR 90SQ045 Schottky diode; heating cycle

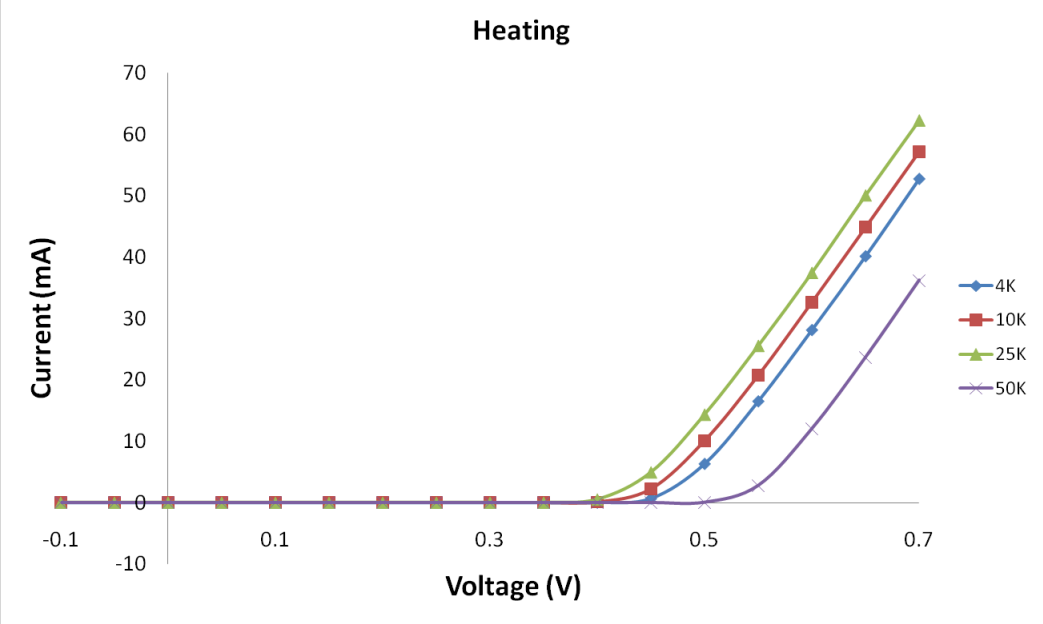

Figure 39: Figure 37 with temperatures from 4 K to 50 K

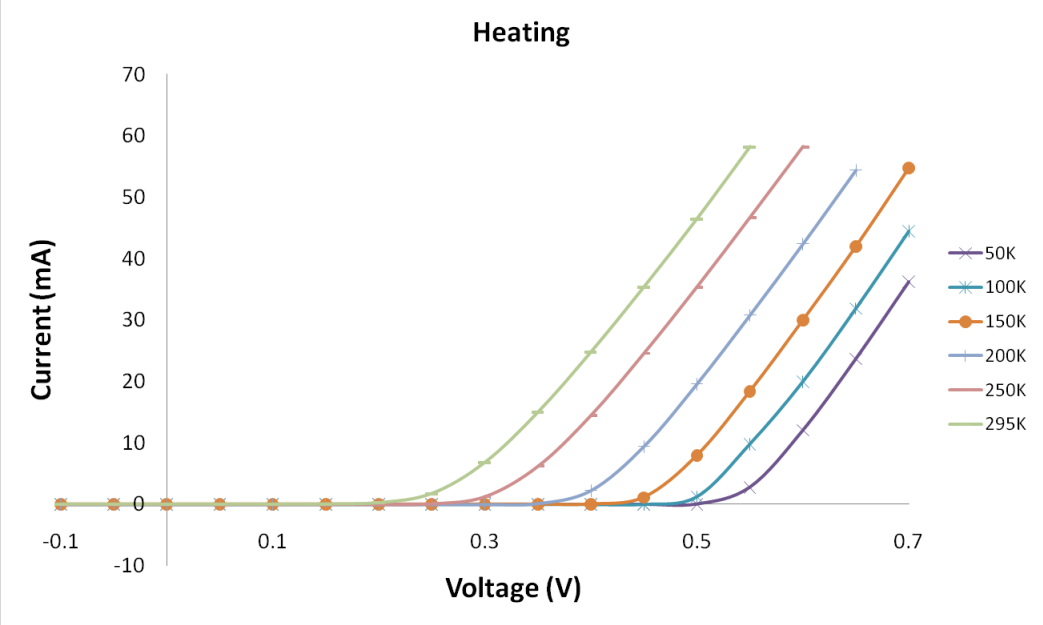

Figure 40: Figure 37 with temperatures from 50 K to 295 K

A hysteresis was observed during the heating cycle. This could be attributed to the charge trapped in the impurity and defect sites. These defect sites can hold the charge for long times thus altering the electric field and the potential in the junction. The diode ideality factors for both cooling and heating cycles were calculated and are listed in Tables 6-7.

Table 6:Diode parameters for the IR 90SQ045 Schottky diode (Cooling cycle)

Temperature	Series Resistance (R_s) (Ohms)	Effective I_o (A/cm^2)	Effective Diode Ideality Factor(η)
295K	4.71	1.8E-06	0.89
250K	4.38	2.4E-08	0.79
200K	4.16	8.0E-11	0.70
150K	4.50	3.5E-15	0.56
100K	4.71	7.3E-22	0.42
50K	4.06	2.1E-30	0.33
25K	4.06	2.0E-28	0.34
10K	4.06	1.8E-24	0.39
4K	3.97	5.0E-21	0.43

Table 7: Diode parameters for the IR 90SQ045 Schottky diode at different temperatures (Heating cycle)

Temperature	Series Resistance (Rs) (Ohms)	Effective Io (A/cm2)	Effective Diode Ideality Factor(n)
4K	3.97	5.05E-21	0.43
10K	4.06	2.03E-16	0.55
25K	4.06	2.0E-28	0.34
50K	3.98	1.37E-28	0.35
100K	3.96	1.07E-25	0.37
150K	3.90	2.72E-20	0.44
200K	4.16	3.63E-16	0.50
250K	4.34	5.59E-11	0.66
295K	4.27	5.48E-09	0.73

In a similar fashion, the current-voltage characteristics of CuPc-Al Schottky diodes with 500 nm long CuPc nanowires of Type-I devices were measured in the temperature range of 4K to 295K. Both cooling (from 295 K to 5 K) and heating (from 4 K to 295 K) cycles were performed. The plots are shown in Figures 41-46. The Schottky diode device parameters were calculated based on thermionic emission theory. It is convenient to divide the characteristics into two regions; the temperature ranges ($T > 50$ K) and ($T < 50$ K). The characteristics in the temperature range (T > 50 K) can be explained by space charge limited current (SCLC) as against tunneling and thermionic currents. When the majority carriers injected by the electrode into the CuPc exceed the thermally generated carriers the SCLC occurs. The SCLC is thought to occur in this device because of two mechanisms; one due to the discrete trappings levels and the second due to the exponential trapping distribution above the valence edge. The SCLC decreases with decreasing temperature down to 50 K. The electrons do not get thermally released from the impurity and defect sites at low temperatures, resulting in space charge which limits the flow of current. At temperatures below 50 K, tunneling dominates and is large enough to cause a net increase in the total current.

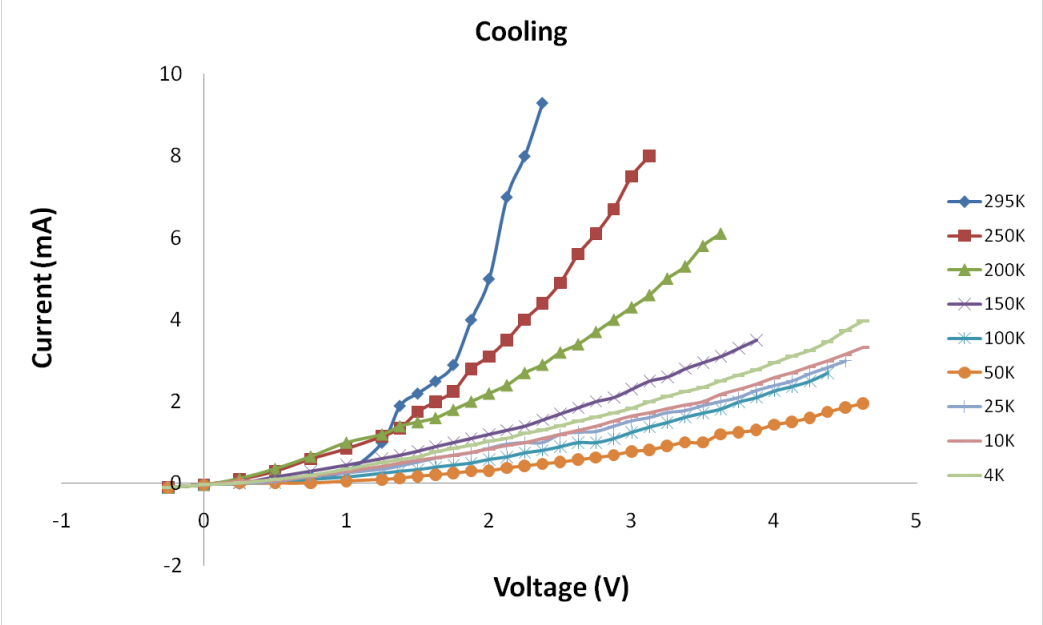

Figure 41: The Low Temperature I-V characteristics of CuPc-Al Schottky diode; cooling cycle

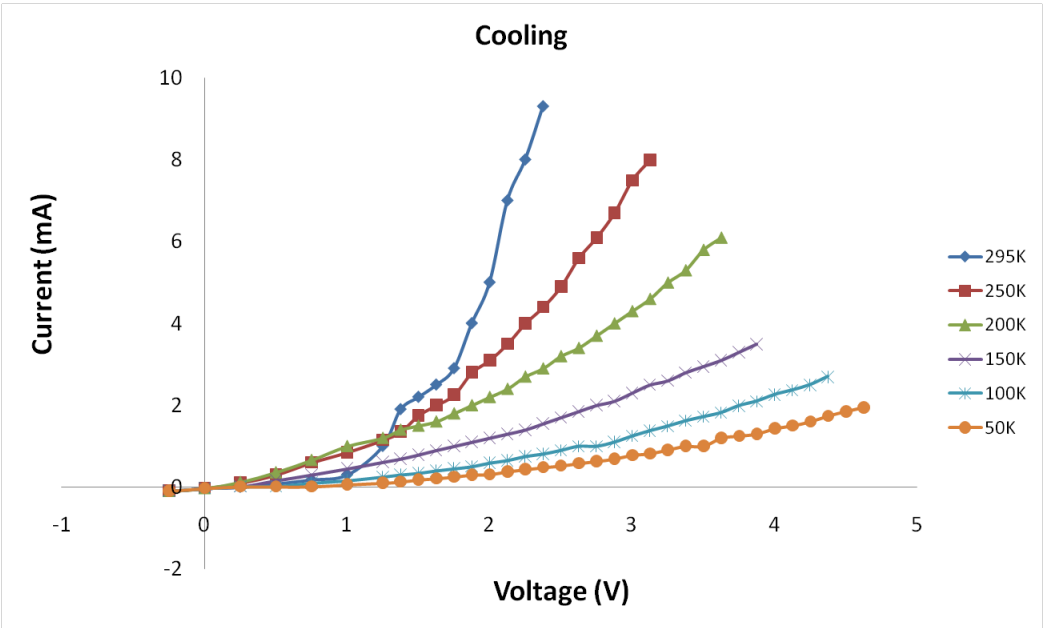

Figure 42: Figure 40 with temperatures from 295 K to 50 K

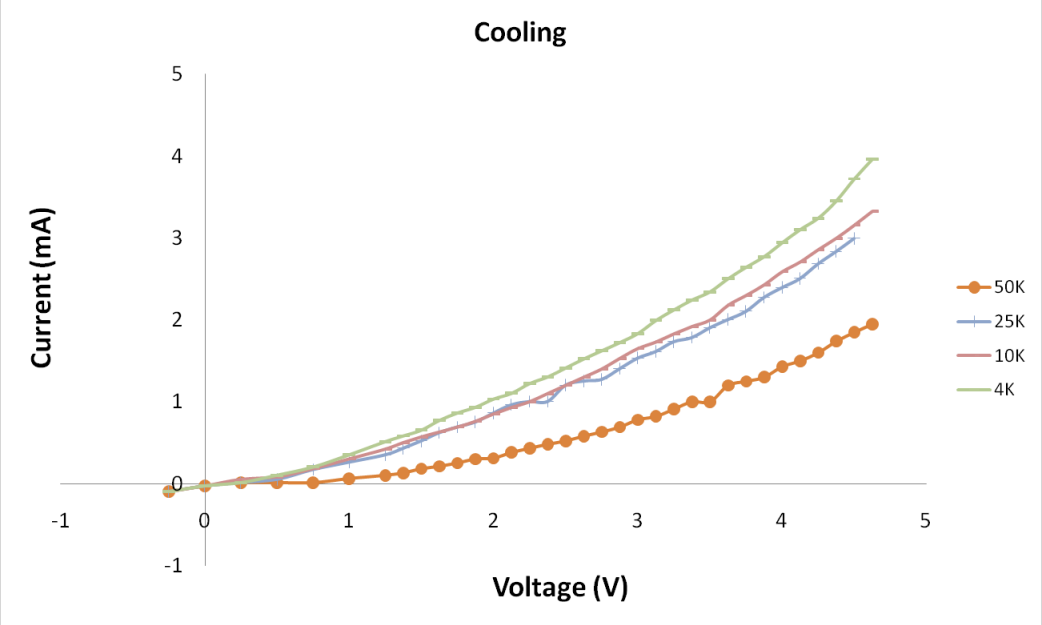

Figure 43: Figure 40 with temperatures from 50 K to 4 K

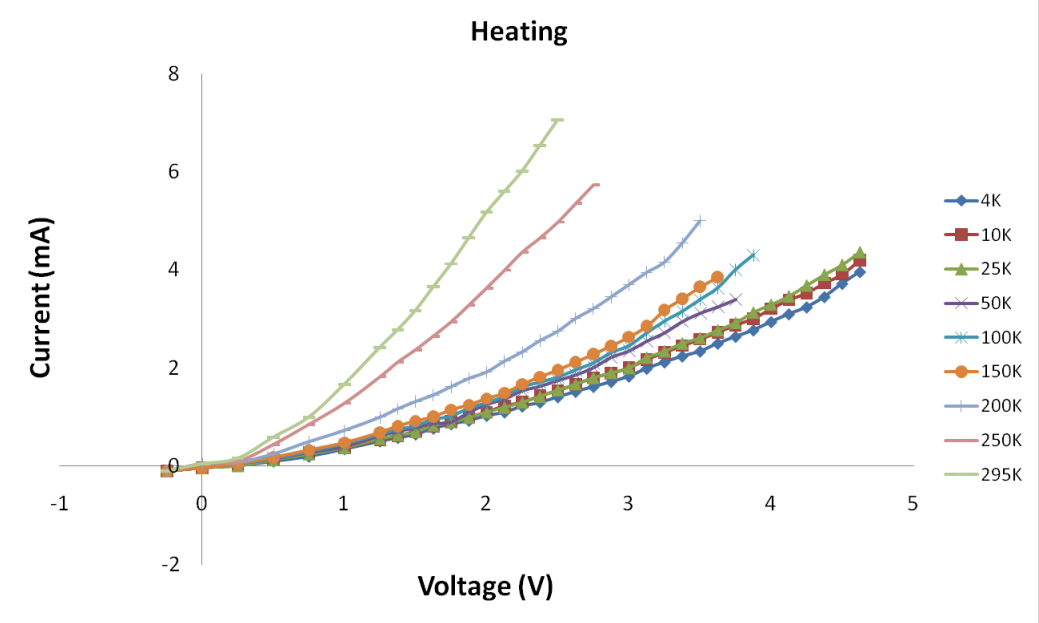

Figure 44: The Low Temperature I-V characteristics of CuPc-Al Schottky diode; heating cycle

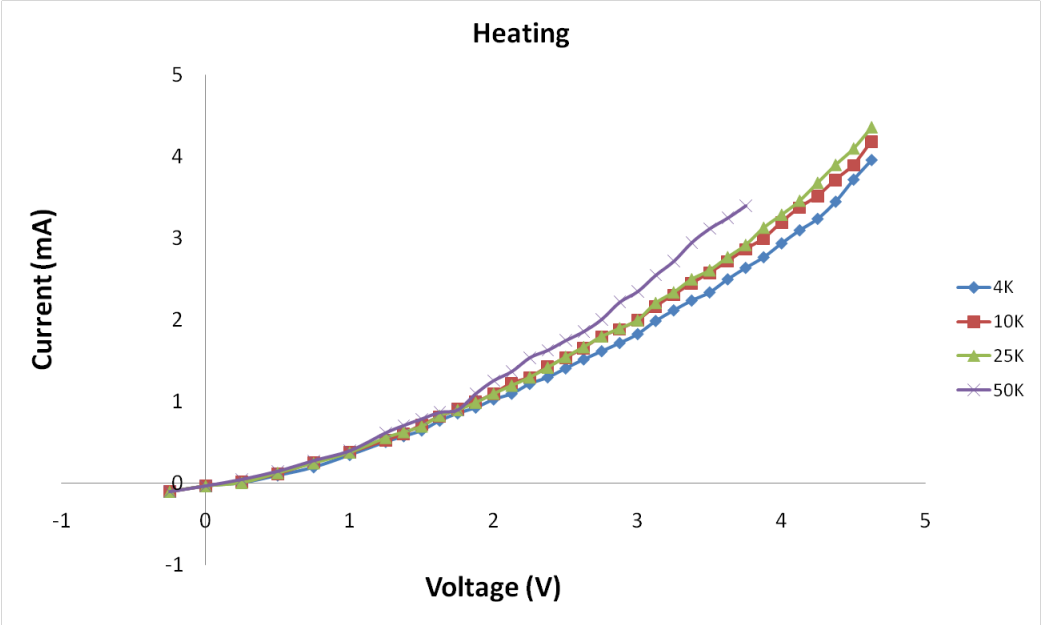

Figure 45: Figure 43 with temperatures from 4 K to 50 K

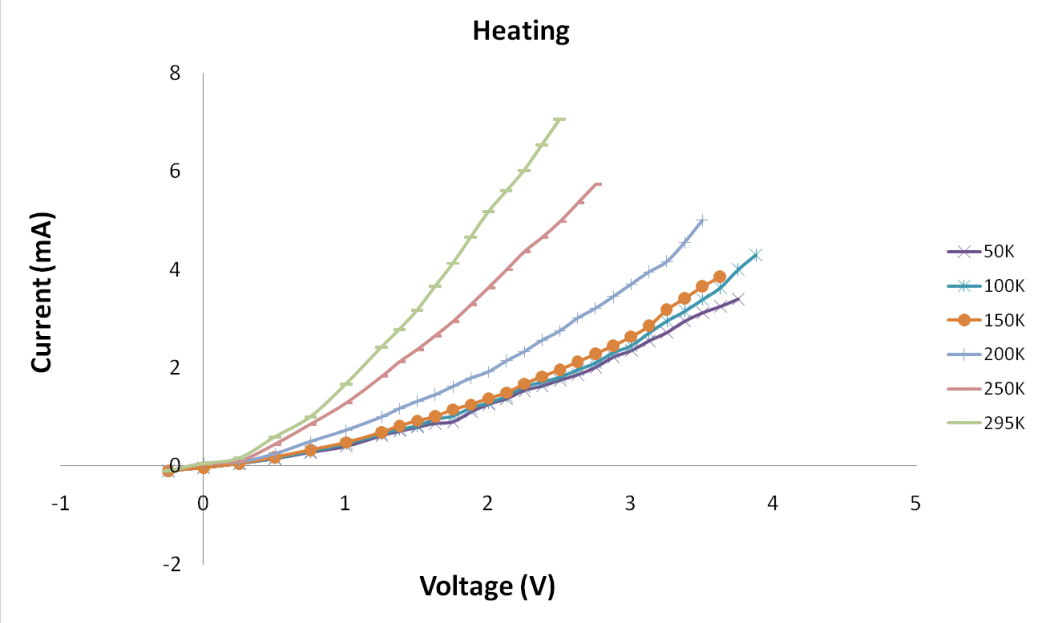

Figure 46: Figure 43 with temperatures from 50 K to 295 K

A hysteresis was also observed in this case. This could be attributed to the fact that the impurity and defect sites trap charges and can hold them for long time, thus altering the electric field and potential at the junction. The calculated diode parameters for cooling and heating cycles are shown in Table 8 and Table 9 respectively. The diode ideality factors vary from 6.8 to 23.3.

Table 8: Diode parameters for the CuPc-Al Schottky diode with 500nm long CuPc nanowires (Cooling cycle)

Temperature	Series resistance (R_s) (Ohms)	Effective I_o (μA/cm^2)	Diode Ideality Factor (η)
295K	96	1.33	6.86
250K	250	62.2	11.99
200K	416	132.68	14.27
150K	625	87.55	18.29
100K	625	20.74	20.59
50K	1250	4.08	14.67
25K	781	34.38	18.41
10K	735	58.41	20.95
4K	520	62.4	23.26

Table 9: Diode parameters for the CuPc-Al Schottky diode with 500nm long CuPc nanowires (Heating cycle)

Temperature	Series resistance (R_s) (Ohms)	Effective I_o (μA/cm^2)	Diode Ideality Factor (η)
4K	520	62.4	23.26
10K	431	90.35	26.89
25K	480	65.06	22.54
50K	833	30.98	10.05
100K	416	80.45	21.17
150K	625	50.96	13.14
200K	595	51.25	8.69
250K	328	72.71	9.73
295K	240	53.23	6.61

5. Conclusions and future prospects

CuPc nanowires were fabricated using electrolytic process. The nanowires were fabricated using two types of AAO templates; AAO over Aluminum tape and AAO over ITO-glass. The nanowires of CuPc electrodeposited in porous alumina templates had the crystallite orientation of the α-phase when annealed below 200^{o}C and transformed into β-phase when annealed at 300^{o}C for 5 hours. β-phase CuPc was observed to have greater absorption at longer wavelengths. Aluminum was used to make a Schottky diode while ITO served as the ohmic contact. Insertion of a thin layer of PEDOT: PSS between CuPc nanowires and the ITO electrode improved the contact and reduced the series resistance by an order of magnitude. It was found that D.C electrodeposition holds good for nanowires of CuPc and pulse electrodeposition for CuPc films. Illumination with "one sun" resulted in higher currents attributed to the photoconductivity of CuPc and the reduction in the junction barrier potential at the CuPc-Al interface. Photovoltaic effect was not observed in the Schottky diodes on the CuPc nanowires. This could be due to the much larger CuPc thickness of 500 nm. The charge transport at low temperatures was dominated by tunneling currents for temperatures below 50 K and by the space charge limiting currents for temperatures above 50 K.

The future work can be focused on electrodepositing CuPc in shorter pores (less than 100 nm long) and check for photovoltaic effect. But, these single layer organic devices deliver quantum efficiencies of less than 1% and power conversion efficiencies of less than 0.1% [27]. The performance of organic photovoltaic devices can be improved by fabricating devices based on donor-acceptor heterojunctions. In our case, lateral heterojunctions can be formed by etching off alumina and replacing it with another organic or inorganic semiconductor. In such structures, almost all excitons formed are close enough to the organic–inorganic interface to be dissociated by electron transfer and all charge carriers have an uninterrupted pathway to the electrodes.

References:

[1] Mitzi D. B., Chondroudis K., Kagan C.R., *IBM: Journal of Research and Development*

[2] *www.wikipedia.com*

[3] Nelson J., Kirkpatrick J., Ravirajan P. 2004 *Phys.Rev. B* **69** 035337

[4] Hill I.G., Schwartz J., Kahn A. 2000 *Org. Electronics* **1** 5

[5] Peumans P., Yakimov A., Forrest S.R. 2003 *J. Appl. Phys*. **93** 3693

[6] Singh V.P., Singh R.S., Parthasarathy B., Aguilera A., Anthony J., Payne M. 2005 *Appl. Phys. Lett.* **86**, 0821061

[7] Singh V.P., Parthasarathy B., Singh R.S., Aguilera A., Anthony J., Payne M. 2006 *Sol. Energy. Mater. Sol. Cells* **90** 798

[8] Tang C.W. 1986 *Appl. Phys. Lett*. **48** 183

[9] Peumans P., Bulovic V., Forrest S.R. 2000 *Appl. Phys. Lett*. **76** 2650

[10] Yakimov A., Forrest S.R. 2001 *Appl. Phys. Lett*. **80** 1667

[11] Kwong C.Y., Djurisic A.B., Chui P.C., Lam L.S.M., Chan W.K. 2003 *Appl. Phy. A* **A77** 555

[12] Xue J.; Rand B.P., Uchida S., Forrest S.R. 2005 *Adv. Mater.* **17** 66

[13] Rajaputra S., Vallurupalli S., Singh V.P. 2007 *J. Mat. Sci.: Mater. Electron*. **18** 1147

[14] Aguilera A., Jayaraman Vivek., Sanagapalli S., Singh R.S., Jayaraman V., Sampson K., Singh V.P. 2006 *Sol. Energy. Mater. Sol. Cells* **90** 713

[15] Singh V.P, Singh R.S., Simpson K. 2006 *Nanostructured Materials for Solar Energy Conversion* ed Tetsuo Soga (Amsterdam: Elsevier) p 167

[16] Rajaputra, S, Sagi, G, Singh V.P., 2008 *Sol. Energy. Mater. Sol. Cells* S0927-0248(08)00115-3

[17] Chandra M. M., Prasad M, 1985, *Phys. Stat. Sol.* **87** K97

[18] Wright J. D., *Encyclopedia of Materials: Science and Technology*, 6986–6991

[19] Xu H.B., Chen H.Z., Xu W.J., Wang M. 2005 *Chem. Phys. Let.* **412** 294

[20] Phok S., Rajaputra S., Singh V.P. 2007 *Nanotechnology* **18** 475601

[21] M. K. Debe, R. J. Poirier, K. K. Kam 1991 *Thin Solid Films* **335** 197

[22] Singh V.P., McClure J.C. 2003 *Sol. Energy. Mater.Sol. Cells*, **76** 3

[23] Rajesh K.R., Verghese S. and Menon C.S., 2007, *Journal of the Physics and Chemistry of Solids*, **68** 556

[24] Jarosz G., 2006 *Journal of Non Crystalline Solids*, **352** 4264

[25] Sze S.M. and Ng Kwok K., 2007 *Physics of semiconductor devices*, Third edition, John Wiley, 157

[26] Zhou Y., Yuan Y., Lian J., Zhang J., Pang H., Cao L., Zhou X., 2006 *Chem. Phys. Let.* **427** 394

[27] Nelson J., 2002 *Mater. Today*, **20** 1369

[28] Kevin M. Coakley, Yuxiang Liu, Chiatzun Goh, and Michael D. McGehee, 2005 MRS Bulletin

[29] Shaheen S.E., Ginley D. S., Jabbour G. E., 2005 *MRS Bulletin*

[30] Lebuna Beegum Shafeek, "Organic-Inorganic heterojunction white light emitting diode".

[31] Antohe S., 2000 *Journal of Optoelectronics and Advanced Materials*, 498

[32] Bozhkov V. G., 2002 *Radiophysics and Quantum Electronics*, 45

Vita

Goutam Chintakula was born in Kakinada, Andhra Pradesh, India on June 9th, 1985. He received his Bachelor of Engineering degree in Electronics and Communication Engineering in 2006 from Osmania University, Hyderabad, India. He worked as a Research Assistant from 2007-2008 in the Electronic Devices Research Group at the University of Kentucky, Lexington, Kentucky, U.S.A.

_____

Goutam Chintakula